J. Plasma Physics (2015), *vol.* 81, 325810107
doi:10.1017/S0022377814000841

A kinetic model of plasma turbulence

S. Servidio[1]†, F. Valentini[1], D. Perrone[2], A. Greco[1], F. Califano[3], W. H. Matthaeus[4] and P. Veltri[1]

[1]Dipartimento di Fisica, Universitá della Calabria, Cosenza, 87036, Italy
[2]LESIA, Observatoire de Paris, 92190 Meudon, France
[3]Dipartimento di Fisica and CNISM, Università di Pisa, Pisa, 56127, Italy
[4]Bartol Research Institute and Department of Physics and Astronomy, University of Delaware, Newark, DE 19716, USA

(Received 31 May 2014; revised 9 September 2014; accepted 10 September 2014; first published online 10 October 2014)

A Hybrid Vlasov–Maxwell (HVM) model is presented and recent results about the link between kinetic effects and turbulence are reviewed. Using five-dimensional (2D in space and 3D in the velocity space) simulations of plasma turbulence, it is found that kinetic effects (or non-fluid effects) manifest through the deformation of the proton velocity distribution function (DF), with patterns of non-Maxwellian features being concentrated near regions of strong magnetic gradients. The direction of the *proper temperature anisotropy*, calculated in the main reference frame of the distribution itself, has a finite probability of being along or across the ambient magnetic field, in general agreement with the classical definition of anisotropy $T_\perp/T_\parallel$ (where subscripts refer to the magnetic field direction). Adopting the latter conventional definition, by varying the global plasma beta (β) and fluctuation level, simulations explore distinct regions of the space given by $T_\perp/T_\parallel$ and $\beta_{||}$, recovering solar wind observations. Moreover, as in the solar wind, HVM simulations suggest that proton anisotropy is not only associated with magnetic intermittent events, but also with gradient-type structures in the flow and in the density. The role of alpha particles is reviewed using multi-ion kinetic simulations, revealing a similarity between proton and helium non-Maxwellian effects. The techniques presented here are applied to 1D spacecraft-like analysis, establishing a link between non-fluid phenomena and solar wind magnetic discontinuities. Finally, the dimensionality of turbulence is investigated, for the first time, via 6D HVM simulations (3D in both spaces). These preliminary results provide support for several previously reported studies based on 2.5D simulations, confirming several basic conclusions. This connection between kinetic features and turbulence open a new path on the study of processes such as heating, particle acceleration, and temperature-anisotropy, commonly observed in space plasmas.

1. Introduction

Turbulence in plasmas is a very difficult problem since it involves interactions between electromagnetic fluctuations and particles, causing phenomena such as dissipation and heating, acceleration mechanisms, temperature anisotropy, particle beam generation and so on (Marsch et al. 1982; Maksimovic et al. 1997; Cranmer et al. 1999; Tu et al. 2002; Bruno and Carbone 2005; Heuer and Marsch 2007; Bale

† Email address for correspondence: sergio.servidio@fis.unical.it

et al. 2009; Bourouaine et al. 2010; Maruca et al. 2011). This complex phenomenology is typically observed in the solar wind, as well as in laboratory settings (Dendy and Chapman 2006; Dendy et al. 2007; Perrone et al. 2013b). The interplanetary gas is a weakly collisional and fully turbulent medium that can be considered as a natural laboratory for plasmas (Bruno and Carbone 2005; Marsch 2006). Even if plasmas in nature are generally turbulent, most of the literature on their kinetic description is based on the linear (or quasi-linear) approach to the Vlasov–Maxwell equations (Gary 1993; Hellinger et al. 2006). However, many hypothesis at the basis of the perturbative approach may be violated, and the plasma dynamics may strongly depart from linear expectations. If requirements and convergence of the ensemble averaging are properly satisfied (Matthaeus et al. 2012), indeed, magnetic fluctuations δb at the largest scales (integrated over several correlation scales) can be on the order of the average magnetic field B_0 (Breech et al. 2008), and also deviation from Maxwellian plasmas are often significant. For example, values of temperature anisotropy may range from 0.1–10 (Kasper et al. 2002). Furthermore, DFs may be very irregular. The latter observational evidence dramatically reduces the validity of perturbative ordering with respect to the Maxwellian velocity distributions, and limits applicability of extensions such as the bi-Maxwellian assumption. Clearly, the full treatment of the velocity space is a very important ingredient in the description of solar wind turbulence.

The difficulty in the simplified treatment of kinetic turbulence raised excitement (and several debates) in the solar wind community (Howes et al. 2008; Matthaeus et al. 2008; Schekochihin et al. 2009; Parashar et al. 2010; Narita et al. 2011; Hunana et al. 2013; Matthaeus et al. 2014). Fluid models as magnetohydrodynamics (MHD) and Hall MHD, as well as Vlasov reduced models such as gyrokinetics, are most accurate when the velocity distribution is close to a Maxwell-Boltzmann distribution. On the other hand, they cannot capture complex velocity space structures nor completely resolve wave-particle effects – situations that can be found in space plasmas. In linear kinetic models of plasma dynamics, moreover, it is expected that the DF deforms manifesting enhanced temperature in the direction parallel (or perpendicular) to the global magnetic field $\boldsymbol{B}_0$, via, for example, resonant ion-cyclotron interaction and Landau resonances (Marsch et al. 1982; Gary 1993; Hollweg and Isenberg 2002; Marsch et al. 2004; Tu et al. 2004; Hellinger et al. 2006). It is not clear how the above phenomena coexist with turbulence, especially in cases in which $\delta b/B_0 \ll 1$, namely the cases of interest for solar wind applications.

The nonlinear regime of the Vlasov model can be investigated numerically, via direct numerical simulations. Particle In Cell (PIC) codes are a widely used approach to numerical simulations of Vlasov plasmas since they require a relatively small computational cost (Birdsall and Langdon 1985; Araneda et al. 2008; Gary et al. 2008; Saito et al. 2008; Araneda et al. 2009; Parashar et al. 2010; Camporeale and Burgess 2011; Daughton et al. 2011; Markovskii and Vasquez 2011b; Parashar et al. 2011; Vasquez and Markovskii 2012; Matteini et al. 2013). On the other hand, the (Lagrangian) PIC schemes are subject to high noise level – a limitation that can be crucial when dealing with short-wavelength turbulence. At very small scales, indeed, the energy level of the fluctuations is typically very low and the intrinsic statistical noise introduced by these algorithms could mask relevant information, unless a very large number of particles is used (for detailed discussions, see Camporeale and Burgess (2011) and Haynes et al. (2014)). In this context, the Eulerian Vlasov approach (described in Sec. 2 below) may overcome these problems, providing a more direct (but numerically expensive) way to describe plasma behavior, especially in the velocity space.

https://doi.org/10.1017/S0022377814000841 Published online by Cambridge University Press

As suggested by hydrodynamic turbulence, intermittency characterizes the turbulent dynamics via, for example, the multifractal behavior of the fluctuations (Vainshtein et al. 1994; Frisch 1995). Vorticity filaments are widely observed in hydrodynamics (Siggia 1981; She et al. 1990; Vincent and Meneguzzi 1991), and can be considered as sharp regions embedded in a highly fluctuating random field. The presence of these structures can therefore affect the statistical properties of the scale-dependent fluctuations, being relevant for turbulent dissipation of energy. Structures have been observed in turbulent flows for a long time: sheets, spirals, and filaments of vorticity represent just few examples. MHD turbulence is also composed of small scale coherent structures that may be sites of enhanced dissipation (Matthaeus and Montgomery 1980; Veltri 1999; Laveder et al. 2013), magnetic reconnection and plasma heating (Parker 1988; Marsch 2006; Sundkvist et al. 2007). However, in low-collisionality plasmas, one expects to find kinetic processes such as temperature anisotropy and energization of suprathermal particles (Gary 1993; Marsch 2006), and in the present work we will investigate the possible link between intermittency and kinetic effects. Hereafter, we will define as 'kinetic effects' all the features that depart from a single-temperature Maxwellian. These involve temperature anisotropy, velocity space fluctuations, particle beams and so on. Given this duality, there are many open questions regarding how a turbulent plasma such as the solar wind dissipates large scale energy and how observed microscopic non-equilibrium conditions are related to the dynamics and thermodynamics that control large scale features. Such small scale dissipative structures, embedded in turbulence, may also be candidates for the process of magnetic reconnection (Servidio et al. 2009; Drake et al. 2010; Osman et al. 2014).

In situ spacecraft measurements reveal that interplanetary proton velocity DFs are anisotropic with respect to the magnetic field (Marsch et al. 1982; Marsch et al. 2004). Recently, there has been intensive research in understanding the organization of solar wind plasma in terms of its kinetic properties (Kasper et al. 2002; Hellinger et al. 2006). In particular, the distribution and evolution of solar wind in a plane described by the parallel plasma beta and the proton temperature anisotropy has motivated several interesting studies (Kasper et al. 2002; Hellinger et al. 2006; Bale et al. 2009; Maruca et al. 2011). Values of the anisotropy $T_\perp/T_\parallel$ range broadly, with most values between 10^{-1} and 10 (Bale et al. 2009; Maruca et al. 2011). The distribution of $T_\perp/T_\parallel$ depends systematically on the ambient proton parallel beta $\beta_\parallel = n_p k_B T_\parallel/(B^2/2\mu_0)$ – the ratio of parallel kinetic pressure to magnetic pressure, manifesting a characteristic shape in the parameters plane defined by $T_\perp/T_\parallel$ and $\beta_\parallel$ (Gary 1993; Bale et al. 2009; Maruca et al. 2011). The general trend with wind expansion towards lower anisotropy and higher parallel beta is understood from adiabatic theory (Hellinger et al. 2006; Matteini et al. 2007), and discussed in terms of the collisional age (Kasper et al. 2008), while the limiting behavior of the distribution may be associated with kinetic instabilities (Hellinger et al. 2006; Bale et al. 2009; Maruca et al. 2011).

More recently (Osman et al. 2012a,b), observations have suggested that a link exists between anisotropy and intermittent current sheets. These studies employed the partial variance of increments (PVI) technique which provides a running measure of the magnetic field intermittency level, and is able to quantify the presence of strong discontinuities (Greco et al. 2008). Elevated PVI values indicate an increased likelihood of finding coherent magnetic structures such as current sheets, and occur in the same regions of parameter space where elevated temperatures are found (Osman et al. 2012a), and also near to identified instability thresholds (Maruca et al. 2011; Osman et al. 2012b). Other observations showed that current sheets are associated with enhanced heating (Osman et al. 2011), while some of the plasma instabilities in

https://doi.org/10.1017/S0022377814000841 Published online by Cambridge University Press

the solar wind seem to develop close to discontinuities (Malaspina et al. 2013). A temporal association of energetic particle fluxes with these coherent structures exists, suggesting that certain mechanisms for suprathermal particles acceleration operate preferentially close to (but not in) magnetic discontinuities (Tessein et al. 2013). HVM and PIC simulations of turbulence complement these findings by establishing that kinetic effects are concentrated near regions of strong magnetic stress (Drake et al. 2010; Servidio et al. 2012; Karimabadi et al. 2013; Perrone et al. 2013a; Wu et al. 2013). Here, we further investigate this path by exploring a broad range of plasma parameters, and establishing a more complex link between temperature anisotropy, turbulence and intermittency. The distinctive distribution of solar wind kinetic parameters is recovered through the combined effects of variation in the initial parameters such as the average plasma beta and the level of fluctuations.

The general picture of plasma turbulence becomes more complicated because of the multi-component nature of the solar wind. The interplanetary medium, although predominantly constituted of protons, is also populated by a finite amount of doubly ionized helium (alpha particles), together with a few percent of heavier ions (Marsch et al. 1982; Hansteen et al. 1997; Bourouaine et al. 2010). Several observations (Marsch et al. 1982; Kasper et al. 2008) have shown that heavier ions are heated and accelerated preferentially as compared to protons and electrons. Moreover, in a recent analysis performed on solar wind data from the Helios spacecraft, the link between kinetic effects and some important parameters of heavy ions, such as relative speed, temperature ratio, and anisotropy, has been investigated by Bourouaine et al. (2010, 2011a,b). Theoretically, the problem of particle heating has also been explained in terms of non-resonant stochastic heating (Dmitruk et al. 2004; Chandran et al. 2010), a mechanism which seems to have a greater efficiency for heavier ions. The non-resonant stochastic heating predictions, moreover, have been further supported by fluid models in which finite Larmor radius corrections are included (Laveder et al. 2011; Hunana et al. 2013).

The paper is organized as follows. In Sec. 2, the governing equations, the numerical algorithm and the parameters will be presented. A brief overview on the statistical properties of the 2.5D simulations will be given in Sec. 3. In Sec. 4, the topological analysis of the velocity DF in plasma turbulence will be presented, while, using the classical choice of describing the velocity space in terms of the magnetic field direction, the analysis of the plane given by $T_\perp/T_{||}$ and $\beta_{||}$ will be the topic of Sec. 5. The role of helium in the plasma dynamics will be reviewed in Sec. 6, while Sec. 7 will be dedicated to the application of the above ideas to spacecraft-like observation of magnetic discontinuities. Preliminary results of the full-dimensional 3D-3V Hybrid Vlasov model will be shown in Sec. 8, where key aspects of the 2D results are confirmed. Finally, conclusions will be discussed in Sec. 9.

2. The model

The Vlasov–Maxwell equations in a hybrid approximation (kinetic ions and fluid electrons) are solved numerically, in a 2D-3V phase-space configuration (Valentini et al. 2007). The basic equations in dimensionless units can be summarized as

$$\frac{\partial f}{\partial t} + \nabla \cdot (\boldsymbol{v} f) + \nabla_v \cdot [(\boldsymbol{E} + \boldsymbol{v} \times \boldsymbol{B}) f] = 0, \tag{2.1}$$

$$\frac{\partial \boldsymbol{B}}{\partial t} = -\nabla \times \boldsymbol{E}, \tag{2.2}$$

https://doi.org/10.1017/S0022377814000841 Published online by Cambridge University Press

$$\boldsymbol{E} = -\boldsymbol{u} \times \boldsymbol{B} + \frac{1}{n}\boldsymbol{j} \times \boldsymbol{B} - \frac{1}{n}\nabla P_e + \eta \boldsymbol{j}, \tag{2.3}$$

where $\boldsymbol{E}$ the electric field, $f(x, y, v_x, v_y, v_z)$ is the ion velocity DF, $\boldsymbol{B} = \boldsymbol{b} + \boldsymbol{B}_0$ the total magnetic field, and $\boldsymbol{j} = \nabla \times \boldsymbol{b}$ the current density. The background magnetic field $\boldsymbol{B}_0$ has been chosen along the z-direction, $\boldsymbol{B}_0 = B_0 \hat{\boldsymbol{e}}_z$ (where $\hat{\boldsymbol{e}}_j$ are unit vectors). The ion density n and bulk velocity $\boldsymbol{u}$ are obtained from the moments of the DF. Quasi-neutrality is assumed, $n \sim n_i \sim n_e$, and an isothermal equation of state for the scalar electron pressure P_e closes the set of hybrid equations (fluid electrons). Numerical instabilities may strongly damage the genuine evolution of turbulence and, in order to suppress spurious numerical effects due to the presence of strong current sheets, a resistive term has been introduced in the Ohm's law ($\eta \boldsymbol{j}$). Note that the electron inertia effects have been neglected in the Ohm's law: the electron skin depth $d_e = \sqrt{(m_e/m_i)} \simeq 0.02$ cannot be resolved with the spatial resolution used in our simulations. In (2.1)–(2.3), time is scaled with the cyclotron frequency Ω_{ci}^{-1}, masses by the ion mass m_i, velocities by the Alfvén speed V_A, and lengths by the ion skin depth $d_i = c/\omega_{pi} = V_A/\Omega_{ci}$ (c is the speed of light and ω_{pi} the ion plasma frequency). In Sec. 8, (2.1)–(2.3) will be adapted to the full-dimensional case (3D+3V).

At $t = 0$ the plasma has uniform constant density and Maxwellian distribution of velocities. Equations are solved in double periodic (x, y) Cartesian geometry, with length $L_{box} = 2\pi \times 20 d_i$. The numerical algorithm used to solve (2.1)–(2.3) is based on the coupling of the splitting method (Chen and Knorr 1976) and the Current Advance Method (Matthews 1994) for the electromagnetic fields, generalized to the hybrid case by Valentini et al. (2007). Double precision is employed, and the initial (Maxwellian) state is perturbed by a 2D spectrum of fluctuations for both magnetic and velocity fields. The initial excited wavenumbers (perpendicular to $\boldsymbol{B}_0$) are chosen with random phases, and the interval of Fourier modes is in the range $[2k_0, 6k_0]$, where $k_0 = 2\pi/L_{box}$. Neither density perturbations nor variances in the z-components are imposed at $t = 0$, namely $\delta n = u_z = b_z = 0$. This is done in order to suppress excessive compressive waves and describe quasi-incompressible turbulence, a case which covers the majority of the solar wind (Matthaeus et al. 1990). The (proton) plasma beta is $\beta = 2v_{ti}^2/V_A^2$, where v_{ti} is the proton thermal speed, and the electron to ion temperature ratio is imposed to be $T_e/T_i = 1$.

We use 512^2 mesh points in physical space and 51^3 in velocity space, so that the 5D phase-space is discretized with $\sim 3.5 \times 10^{10}$ grid points. The velocity space resolution is varied for the simulations with smaller plasma beta, where we tested the results by varying the resolution from 51^3–81^3. No difference has been found between the above cases, confirming that filamentation-instabilities, in the velocity space, are not significantly influencing the results for the parameters we used. The limits of the velocity domain in each direction are fixed at $v^{\max} = \pm 5 v_{ti}$. The resistivity is chosen to be $\eta = 1.7 \times 10^{-2}$. This value is small enough to achieve reasonably high Reynolds numbers while ensuring adequate spatial resolution; this quantity is however not intended to model any specific plasma process. With a time step of $\Delta t = 0.01$, the conservation of the total mass, energy and entropy of the system is satisfied with typical relative errors of $\sim 10^{-5}\%$, $10^{-3}\%$, and $10^{-1}\%$, respectively.

We report on different simulations, varying both the plasma beta and the level of turbulence. Six values of β were considered, namely $\beta = 0.25$, 0.5, 1, 1.5, 2, 5, with $\delta b/B_0 = 1/3$. Two other simulations have been performed varying the level of fluctuations, namely with $\beta = 0.25$, 1.0 with $\delta b/B_0 = 2/3$. Here $\delta b = \langle b_x^2 + b_y^2 \rangle$ (at $t = 0$), where $\langle \bullet \rangle$ denote spatial averages. Data from simulations are labeled as Run

https://doi.org/10.1017/S0022377814000841 Published online by Cambridge University Press

Run	1	2	3	4	5	6	7	8
$\delta b/B_0$	1/3	1/3	1/3	1/3	1/3	1/3	2/3	2/3
β	0.25	0.50	1.00	1.50	2.00	5.00	0.25	1.00
$t^\star(\Omega_{ci}^{-1})$	38	38	38	38	38	38	10	15

TABLE 1. Parameters of the Runs: the initial level of magnetic fluctuations $\delta b/B_0$, the plasma β, and the time $t^\star$ of the maximum of $\langle j_z^2 \rangle$, which indicates the peak of nonlinear activity.

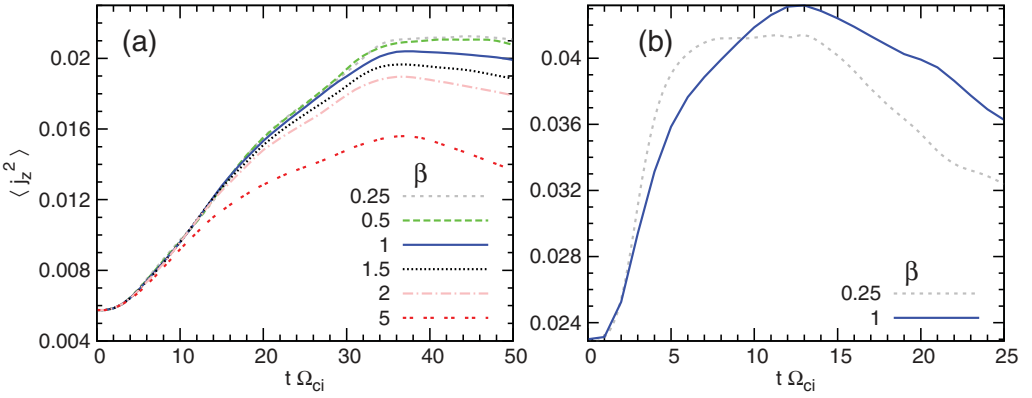

FIGURE 1. The level of turbulent activity $\langle j_z^2 \rangle$ for Run 1–6 (a) and Run 7–8 (b). See Table 1 for more details about the simulations.

1, 2, . . . , 8, respectively, and details on the simulations are summarized in Table 1. With this variety of conditions most of the solar wind cases are covered, going from compressible to almost-incompressible regimes, from weakly- to average-anisotropic plasma regimes. We expect that, in the turbulent regime, kinetic effects develop simultaneously within the cascade (Servidio et al. 2012). In each of these regions, kinetic effects may play a fundamental role in the production of interesting features, such as accelerated suprathermal particles, temperature anisotropy, wave-particle like interactions, and the formation of beams in the ion DF.

3. Statistical properties of kinetic turbulence

In our numerical experiments turbulence is decaying, namely energy is carried from large to small scale via nonlinear interactions, and then is dissipated at small scales, through both kinetic and resistive effects. It is important to quantify in this case the level of turbulence and its time evolution. In analogy with MHD models, in decaying turbulence there is an instant of time, let say $t^\star$, at which the turbulent activity is maximum (Mininni and Pouquet 2009), and which is identified as the peak of the mean squared current density $\langle j_z^2 \rangle(t)$ (where brackets denote spatial averages.) The out-of-plane current j_z is a good measure of the small scale activity, analogously to the vorticity for 2D hydrodynamics (Biskamp 2003; Servidio et al. 2012). The average current, shown in Fig. 1 for all the runs, reaches a maximum value and then slowly decays, approaching eventually zero for $t \to \infty$. At the time of the maximum current, which in the collisional cases corresponds to the peak of dissipation, the system shares many similarities with stationary and statistically homogeneous turbulence. This time $t^\star$ is reported for each Run in Table 1. As it can be noticed from Fig. 1(a), the value of

https://doi.org/10.1017/S0022377814000841 Published online by Cambridge University Press

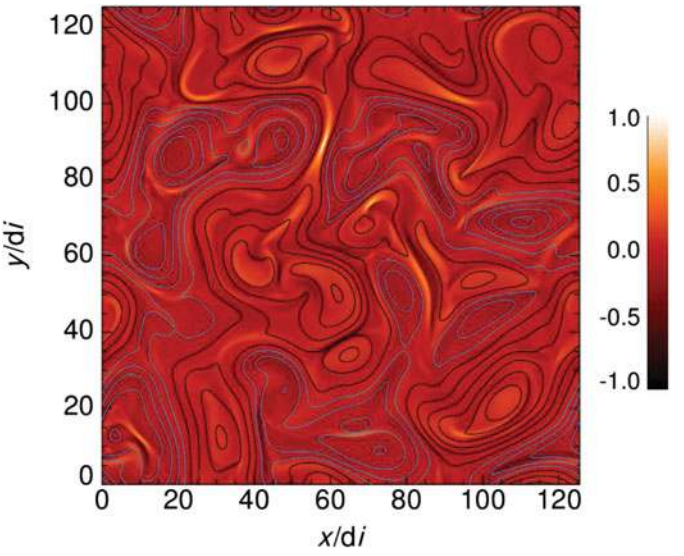

FIGURE 2. Shaded contours of the current density j_z and line contours of the magnetic potential a_z, for Run 5 ($\beta = 2$ and $\delta b/B_0 = 1/3$). The field topology is characterized by magnetic islands and current sheets, as expected in 2D turbulence.

the plasma β slightly influences the maximum current: $\langle j_z^2 \rangle$ is lower at higher β. This may indicate that the in-plane dynamics is more suppressed in the cases of higher beta, probably due to the disappearance of fast magnetosonic activity. For the cases with higher level of fluctuations (Runs 7 and 8), as can be noticed in Fig. 1(b), the meta-stationary state is reached earlier, and the level of current is obviously higher.

For Run 5, we report in Fig. 2 the contour plot of $j_z(\boldsymbol{x})$, together with the line contours of the magnetic potential a_z, where $\boldsymbol{b}_\perp = \nabla a_z \times \hat{\boldsymbol{z}}$. Different runs have similar behavior (not shown here). Turbulence manifests through the appearance of coherent structures, exhibiting vortices and current sheets of various size. In between islands, j_z is narrow and intense, being a signature of the intermittent nature of the magnetic field (Matthaeus and Montgomery 1981; Wu and Chang 2000; Bruno and Carbone 2005; Kiyani et al. 2009). In these regions of high magnetic stress, as we will see later, reconnection locally occurs at the X-points of a_z (Servidio et al. 2009, 2010; Drake et al. 2010; Haynes et al. 2014). From a qualitative analysis, the size of these current sheets is on the order of few d_i's. Note that these also manifest a bifurcation, typical signature of the Hall effect (Shay et al. 1998; Donato et al. 2012). The pattern is similar for all the values of β, except that the value of the current density decreases at high β, as can be evinced by Fig. 1(a).

As expected for plasma turbulence, β plays an important role on the nature of the fluctuations, and, in particular, on the compressibility of the system. In Fig. 3, density fluctuations, computed as $\delta n = n - \langle n \rangle$, are compared for two different runs, namely $\beta = 0.25$ (Run 1) and 5 (Run 6). In the first case the level of density fluctuations is higher, consistent with the dominance of magnetosonic activity: in some regions fluctuations can manifest strong compressions, with deviations from the average of $\sim$50%. Moreover, compared to the very high beta plasmas [panel (b) of the same figure], the density shows much steeper and well-defined gradients, possibly related to the existence of shock-like structures. These fluctuations may also indicate local

https://doi.org/10.1017/S0022377814000841 Published online by Cambridge University Press

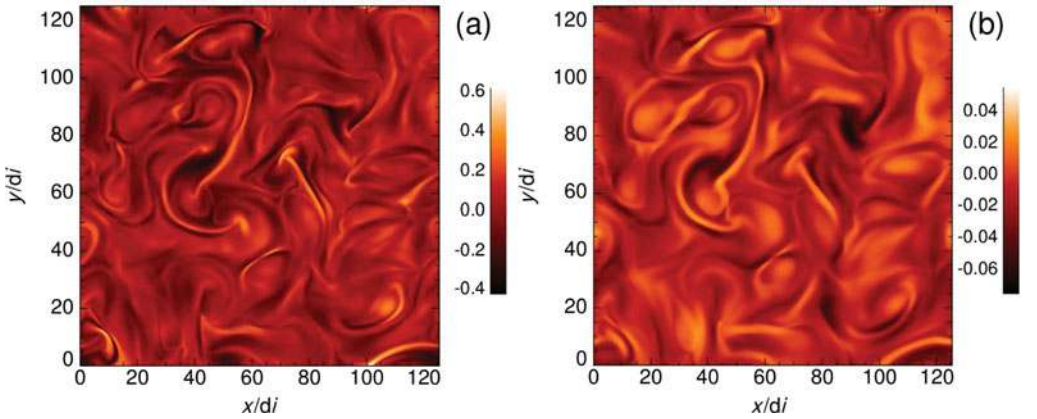

FIGURE 3. Density fluctuations δn for $\beta = 0.25$ (a) and 5 (b). The cases correspond to Runs 1 and 6, in Table 1. The level of fluctuations, as expected, strongly depends on β.

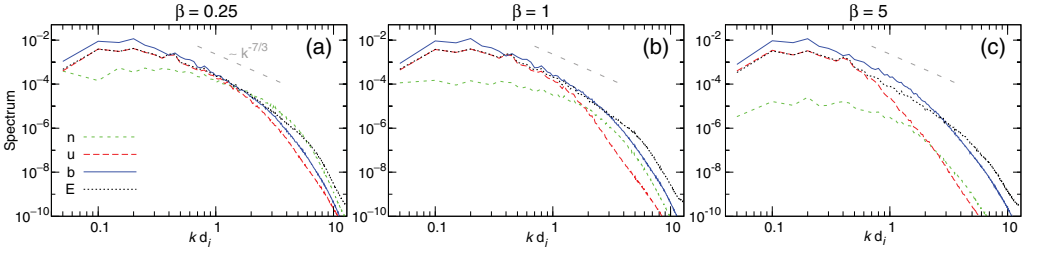

FIGURE 4. Spectra of the ion density (green thin-dashed), ion bulk velocity (red thick dashed), magnetic field (blue solid) and electric field (black dot-dashed), for $\beta = 0.2$ (a), 1(b), and 5(c). The power law $k^{-7/3}$ (gray long-dashed) is reported just as a reference.

patterns of fast magnetosonic (whistler) activity, which is damped at high β (Davidson 1990; Servidio et al. 2007).

To better quantify turbulence, we computed the Fourier spectra of the density n, the ion bulk velocity $\boldsymbol{u}$, the magnetic $\boldsymbol{b}$ and the electric $\boldsymbol{E}$ fields. These omni-directional spectra are shown as a function of kd_i in Fig. 4, for $\beta = 0.25$, 1 and 5. For all the cases, the large scale activity is essentially incompressible, that is $|n_k|^2$ is quite low at small wavenumbers. This effect is commonly observed in space plasmas (Bruno and Carbone 2005), in which large scale density variations are typically limited to those imposed by boundary constraints. It is important to note, as previously discussed, that the level of density fluctuations decreases with increasing β. At small β, moreover, the density spectrum is more broad and exhibits an inertial range.

The Alfvén effect (Dobrowolny et al. 1980), or expected near-equipartition of energy in the magnetic and the velocity fields, is typical of MHD turbulence, and can be seen in the inertial range of Fig. 4, namely at scales $0.2 < kd_i < 2$. This near-equipartition of energy however is broken at the ion skin depth (Alexandrova et al. 2008), typical of both kinetic and dispersive fluctuations (Bale et al. 2005; Valentini et al. 2008; Alexandrova et al. 2009; Sahraoui et al. 2009; Markovskii and Vasquez 2011b; Servidio et al. 2012). Similarly to solar wind observations (Bale et al. 2005), we remark that the electric field activity at larger wavenumbers is higher than the magnetic activity, possibly due to the Hall effect (Matthaeus et al. 2008). Note that, although resolution in Vlasov simulations is not generally enough to guarantee

https://doi.org/10.1017/S0022377814000841 Published online by Cambridge University Press

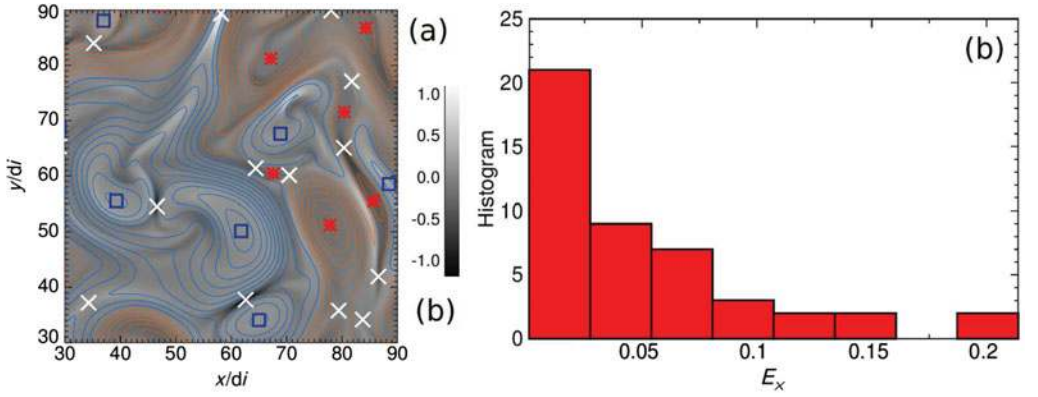

FIGURE 5. (a) Iso-lines of the magnetic potential a_z, shaded contour of the current density j_z, and the position of the critical points: O-points (blue squares for the maximum and red stars for the minimum) and X-points (white $\times$). Only a portion of the entire simulation box is shown. (b) Histogram of the reconnection rates.

definitive statements about scaling laws (Matthaeus et al. 2008), the spectral slope is consistent with the scaling of $k^{-7/3}$, which is very close to several theoretical predictions, such as in Hall MHD and in the so-called Kinetic Alfvén turbulence (Bale et al. 2005; Galtier and Buchlin 2007; Howes et al. 2008; Sahraoui et al. 2009; Schekochihin et al. 2009; Alexandrova et al. 2013).

3.1. *Magnetic reconnection in Vlasov turbulence*

As described by Servidio et al. (2009), in order to understand the magnetic field topology we analyzed $a_z(x, y)$ (Biskamp 2000). The square Hessian matrix of a_z is $H^{a_z}_{i,j}(\boldsymbol{x}) = \frac{\partial^2 a_z}{\partial x_i \partial x_j}$. At each neutral point, $\nabla a_z = 0$, we compute the eigenvalues of $H^{a_z}_{i,j}$. If both eigenvalues are positive (negative), the point is a local minimum (maximum) of a_z (an O-point). If the eigenvalues are of mixed sign, it is a saddle point (an X-point). Figure 5(a) shows an example of the magnetic potential (only a fraction of the entire box) with its critical points (for Run 5, for example, the number of X-points is $\sim$50.) Many magnetic islands are present, and, at the boundaries of these vortices, the electric field is bursty.

The reconnection rates of the in-plane magnetic field are computed as the rate of change of the magnetic flux through $\dot{a}_z$, and using the electric field at the saddle points,

$$\frac{\partial a_z}{\partial t} = \eta j_z|_{X-\text{point}} = -E_\times, \tag{3.1}$$

where $E_\times$ is an abbreviation for the electric field measured at the X-point. The reconnection rates have been normalized to the mean square fluctuation δb^2, appropriate for Alfvènic units. In Fig. 5(b) the histogram of the absolute value of the reconnection rate is shown, revealing that the distribution is quite broad, with a condensation near very low reconnection rates. The strong variations from the average suggest that there are few values of $E_\times$ that exceed the typical fast reconnection limit of $E_\times \sim 0.1$, as it can be seen in Fig. 5(b). Note that the rates are slightly lower than the MHD and Hall MHD cases (Servidio et al. 2009; Donato et al. 2012). This effect may be due to the much lower resolution of the kinetic simulations – kinetic physics requires much expensive computational resources. Higher resolution simulations, as well as the full kinetic treatment of electrons will be investigated in

https://doi.org/10.1017/S0022377814000841 Published online by Cambridge University Press

the future, exploring the possibility of very fast collisionless reconnection events (Birn et al. 2001), that in this case are part of turbulence itself.

4. Local analysis of the distribution function

In this section, we propose an alternative point of view on the description of plasma turbulence, showing that the proton DF is modulated by the local magnetic field, in a complex way. A statistical description of the link between the magnetic skeleton of turbulence and the velocity sub-space of the DF is performed. For this purpose we will make use of a single simulation, namely Run 5 (see Table 1), for which $\beta = 2$ and $\delta b/B_0 = 1/3$. As shown by Servidio et al. (2012), simulations with different box size and level of turbulence give similar results, although they produce different levels of anisotropy. An overview of the dependency of kinetic effects on β and $\delta b/B_0$ is given in Sec. 5.

The presence of current in sheet-like structures, observed in Figs. 2 and 5(a), suggests the possibility that kinetic effects may be inhomogeneous as well. To confirm this hypothesis, we quantify kinetic effects looking directly at the high-order velocity moments of the DF. In particular, we will concentrate on the temperatures of f, that for a Maxwellian must be 1 (in these units). The preferred directions of f in the velocity space, for each $\boldsymbol{x}$, can be obtained from

$$A_{ij}(\boldsymbol{x}) = \frac{1}{n}\int (v_i - u_i)(v_j - u_j) f \; d^3v. \tag{4.1}$$

The above tensor can be studied in a diagonal form computing its eigenvalues $\{\lambda_1, \lambda_2, \lambda_3\}$ and the respective normalized eigenvectors $\{\hat{\boldsymbol{e}}_1, \hat{\boldsymbol{e}}_2, \hat{\boldsymbol{e}}_3\}$, that represent a proper reference frame (Sonnerup and Cahill 1967). Note that λ_i are the temperatures (for convention we choose $\lambda_1 > \lambda_2 > \lambda_3$) and $\hat{\boldsymbol{e}}_i$ the anisotropy directions. For a Maxwellian, the tensor in (4.1) is diagonal and degenerate ($\lambda_i = 1$ and no preferred direction.) Using this eigensystem, the *proper temperature anisotropy* is given by λ_1/λ_3. The anisotropy, whose shaded contour is represented in Fig. 6(a), is confined in sheet-like structures, modulated by the local magnetic field: anisotropy is low inside magnetic islands while is high near current sheets. These are regions of strong magnetic stress, shifted away from the X-points.

The PDF of λ_1/λ_3 [see Fig. 6(c)], evaluated at $t^\star$ sampling over the entire domain of the simulation, shows that f is not isotropic, with several events reaching strong anisotropy ($\lambda_1/\lambda_3 \sim 1.7$). As reported by Servidio et al. (2012), a comparison between simulations reveals that higher level of turbulence produces patches with higher anisotropy. In addition, the system size influences the anisotropy phenomenon – smaller systems are slightly more anisotropic. The latter is due to the fact that kinetic effects are more active when the system size is comparable to d_i. It is evident that the main ingredient that enhances anisotropy is turbulence.

At this point it is interesting to further characterize the deformations of the DF, through a more general analysis. Theoretical models of plasmas tend to simplify the velocity DF as simple bi-Maxwellians, namely assuming that the distribution has only two main temperatures, one of which is strictly aligned with the ambient magnetic field. The DF shows, instead, a strong non-gyrotropic character and a much more complex structure in the velocity space. To quantify the *non-gyrotropy*, we measured the ratio of the middle and the smallest eigenvalues, namely λ_2/λ_3. For the gyrotropic case, this value should be uniformly equal to unity, while here, in the full Vlasov treatment, we observe that this *secondary anisotropy* can cover a very broad range. In

https://doi.org/10.1017/S0022377814000841 Published online by Cambridge University Press

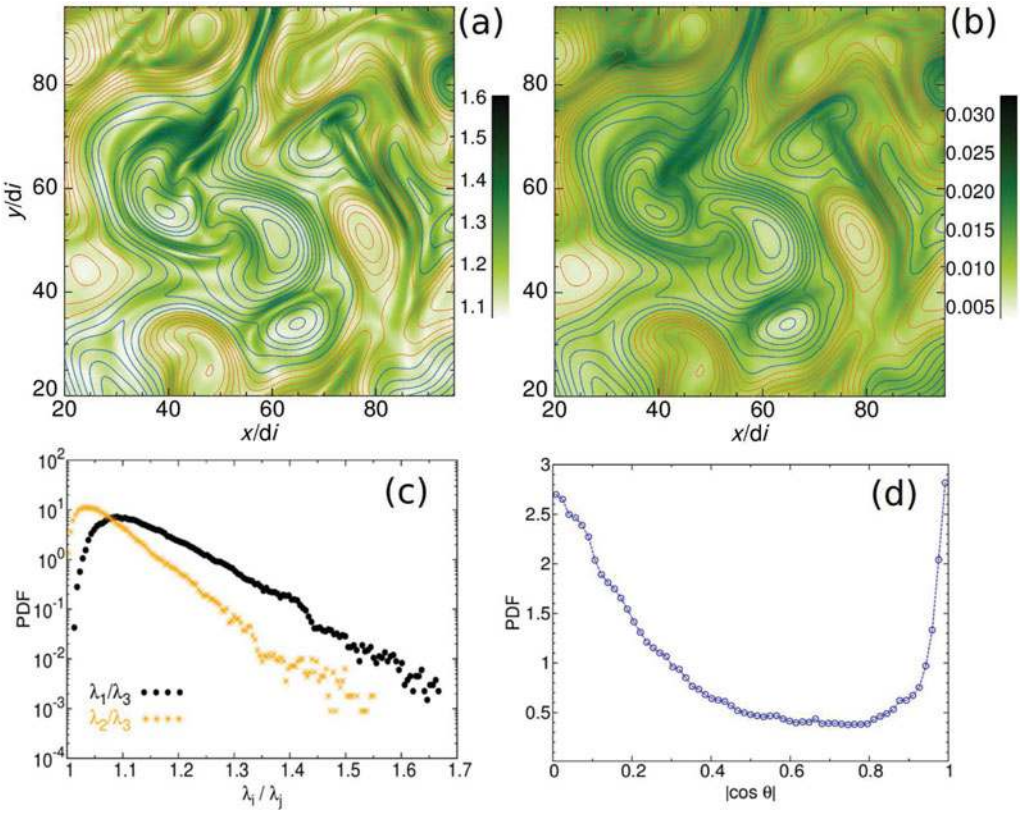

FIGURE 6. (a) Shaded contour of the proper anisotropy λ_1/λ_3 together with the in-plane magnetic field lines; (b) Shaded contour of ϵ defined by (4.3); (c) PDF of the main temperature anisotropy λ_1/λ_3 (black bullets) and the secondary anisotropy λ_2/λ_3 (orange stars); (d) PDF of the cosine-angle given by (4.4).

Fig. 6(c), in fact, it can be observed that this secondary anisotropy can reach quite large values, raising some questions on the validity of simplified models of kinetic plasma turbulence.

Apart of (4.1), other moments can contribute to the departure from the Maxwellian condition. Non-thermal behavior of the plasma may be revealed by local comparison of the DF with the corresponding Maxwellian. At each position in space $\boldsymbol{r}$, the associated Maxwellian distribution g can be computed as

$$g(\boldsymbol{r}, \boldsymbol{v}) = C \ \exp\left[-\frac{1}{2T} \sum_j (v_j - u_j)^2 \right], \tag{4.2}$$

where u_j is the bulk velocity, T is the isotropic temperature in that point, and C is a normalization constant that varies in space and depends on density and temperature. At a given position $\boldsymbol{r}$, when kinetic effects develop, f differs from g and these departures can be quantified as (Greco et al. 2012)

$$\epsilon(\boldsymbol{r}) = \frac{1}{n} \sqrt{\int (f - g)^2 \ d^3v}. \tag{4.3}$$

https://doi.org/10.1017/S0022377814000841 Published online by Cambridge University Press

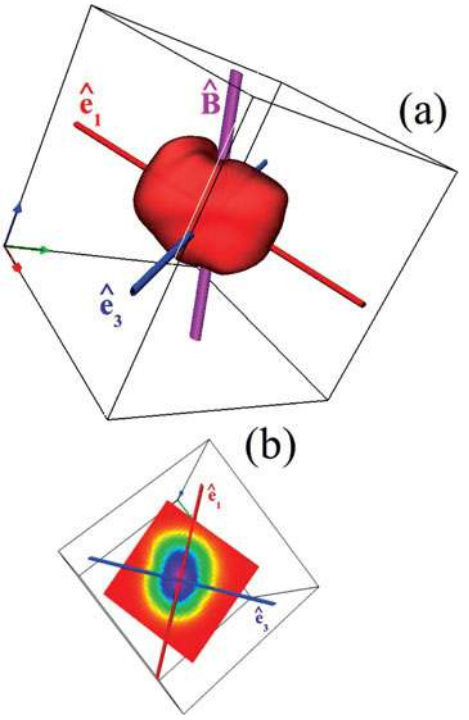

FIGURE 7. (a) Isosurfaces (red) of the velocity DF $f(\boldsymbol{v})$, at a given spatial position. (b) Two-dimensional cut of f in the minimum variance frame. Thin (red) and thicker (blue) axis indicate $\hat{\boldsymbol{e}}_1$ and $\hat{\boldsymbol{e}}_3$, respectively. The magnetic field direction $\hat{\boldsymbol{B}}$ is represented with a thick (magenta) tube.

As it can be seen from Fig. 6(b), ϵ is non-uniform and limited in narrow regions of the space, where non-thermal effects are concentrated. The quantity ϵ may differ from zero because of various distortions of f – for example, it can be due to anisotropy, to non-zero skewness (heating flux), or to high (low) kurtosis of f. Further applications of this quantity to solar wind-like observation will be presented in Sec. 7.

It is now interesting to examine the structure of the DF in the presence of turbulence. Since HVM models do not suffer from any lack of statistics in the velocity space, here we provide an example of f, at a given $\boldsymbol{x}$. In Fig. 7(a), the isosurfaces of f reveal that the DF is strongly affected by the presence of turbulence, resembling a potato-like structure elongated in the $\hat{\boldsymbol{e}}_1$-direction ($\hat{\boldsymbol{e}}_3$ and the direction of the local magnetic field $\hat{\boldsymbol{B}} = \boldsymbol{B}/|\boldsymbol{B}|$ are reported as well). In the same figure (panel b), a slice in the $\hat{\boldsymbol{e}}_1 - \hat{\boldsymbol{e}}_3$ plane is reported, showing that elongation along $\hat{\boldsymbol{e}}_1$ is balanced by a squeezing (depression) along $\hat{\boldsymbol{e}}_3$.

As can be immediately noticed from Figs. 7 and 6(c), the preferred axis $\hat{\boldsymbol{e}}_1$ may depart from the magnetic field direction $\hat{\boldsymbol{B}}$, having a distribution of angles with the magnetic field. Since turbulence is a cross-scale effect, a statistical approach is required. To establish how the DF *chooses* its main axis, we computed, at each spatial position $\boldsymbol{x}$, the cosine-angle between $\hat{\boldsymbol{e}}_1$ and the unit vectors of the magnetic field (Kerr 1987),

$$\cos\theta(\boldsymbol{x}) = \hat{\boldsymbol{e}}_1(\boldsymbol{x}) \cdot \hat{\boldsymbol{B}}(\boldsymbol{x}). \tag{4.4}$$

Note that if $\hat{\boldsymbol{e}}_1$ and $\hat{\boldsymbol{B}}$ are spatially random and uncorrelated fields, the distribution of the cosine-angles should be flat and, in particular, PDF($|\cos\theta|$) ~ 1. For the cases

https://doi.org/10.1017/S0022377814000841 Published online by Cambridge University Press

in which the magnetic field and the main axis are strictly parallel and perpendicular, Dirac distributions peaked at $|\cos\theta| = 1$ and $|\cos\theta| = 0$ should be observed, respectively. The PDF of (4.4) is reported in Fig. 6(d), showing that, although the local magnetic field provides on average the two main directions, a significant population is present at all the angles, suggesting that the main axis of f is determined by the magnetic field in a complex way: $\hat{\boldsymbol{e}}_1$ can be both along or across $\boldsymbol{B}$, or either at oblique angles (but with less probability). These results underline some difficulties in imposing the magnetic field as the unique axis of deformations and suggest that, using the standard definition of temperature anisotropy, together with the bi-Maxwellian approximation, may lead to an underestimation of kinetic effects.

5. Proton temperature anisotropy

Statistical analysis of solar wind data relates proton temperature anisotropy $T_\perp/T_\parallel$ and parallel plasma beta $\beta_\parallel$, where subscripts refer to the local magnetic field direction. In this Section, we will recover this relationship using the ensemble of HVM simulations presented before. By varying plasma parameters, such as the global plasma beta and fluctuation level, we observed that simulations explore distinct regions of the space given by $T_\perp/T_\parallel$ and $\beta_\parallel$, similar to solar wind sub-datasets. Moreover, both simulations and solar wind data suggest that temperature anisotropy is not only associated with magnetic intermittent events, but also with gradient-type structures in the flow and in the density. This connection between non-Maxwellian kinetic effects and various types of intermittency may help to understand the complex nature of plasma turbulence.

For each simulation in Table 1, we used the classical measure of the temperature anisotropy as a function of the $\beta_\parallel$, where the direction is given by the local magnetic field. In Fig. 8(a) we show the two-dimensional PDF (or joint distribution) of anisotropy versus $\beta_\parallel$, for the case with $\beta = 0.5$ and $\delta b/B_0 = 1/3$ (Run 2), at the peak of nonlinear activity. Similarly to λ_1/λ_3, a large spread is observed (note that, at $t = 0$, $T_\perp/T_\parallel = 1$), with a concentration around $\beta_\parallel \sim 0.5$ and $T_\perp/T_\parallel \sim 1$. As it can be seen from the direct comparison with the solar wind, reported in Servidio et al. (2014), for each solar wind interval, the picture of the anisotropy distribution is very similar, revealing that turbulence plays a major role in the particular area occupied by the distribution. In Fig. 8 [panel (b)], the distributions are compared for different simulations. Varying over values of β, with initial $\delta b/B_0 = 1/3$, most of the area is covered. It is apparent that the dynamically evolved data are strongly modulated by the choice of the average beta. Notably, the resulting distributions resemble the familiar form of those accumulated from years of solar wind data (Bale et al. 2009; Osman et al. 2012b).

To examine the influence of the turbulence level we performed two more simulations in which we varied the level of fluctuations. In Fig. 9, we compare PDFs of simulations with $(\beta, \delta b/B_0) = (0.25, 1/3)$ and $(0.25, 2/3)$ (Run 1 and 7), and $(1, 1/3)$ with $(1, 2/3)$ (Runs 3 and 8). It is evident that the level of fluctuations, together with the mean plasma beta, strongly influences the distribution of anisotropies in Vlasov turbulence. Note that in the same figure, theoretical predictions for the linear Vlasov instabilities are also reported (Kasper et al. 2002; Hellinger et al. 2006). A similar analysis conditioning on the turbulence level has been carried out for solar wind, sampling the data for both β and $\delta b/B_0$ (Servidio et al. 2014). The comparison shows a good agreement between simulations and observations. We can clearly discern that the level of fluctuations plays a direct role in spreading the distribution of

https://doi.org/10.1017/S0022377814000841 Published online by Cambridge University Press

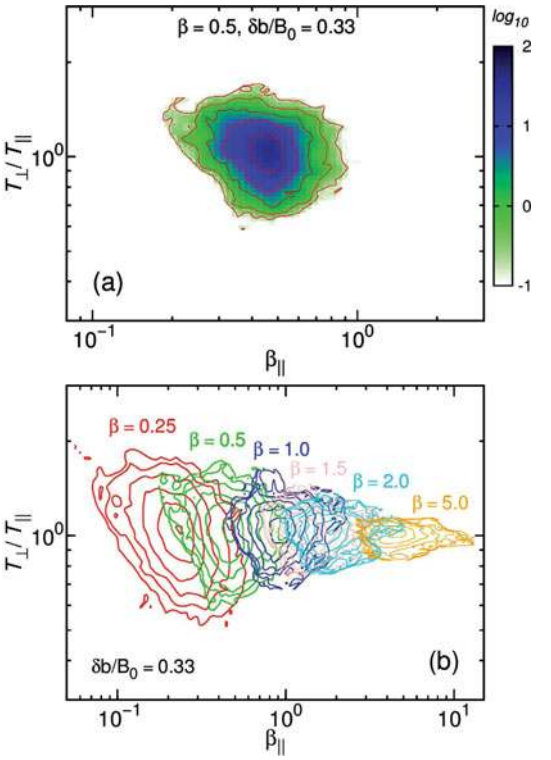

FIGURE 8. (a) Two-dimensional PDF (or joint distribution) of the anisotropy against $\beta_{\|}$, for the simulation with average $\beta = 0.5$ and $\delta b/B_0 = 1/3$ (Run 2); (b) Comparison of the joint distributions for simulations with $\delta b/B_0 = 1/3$ and $\beta = 0.25, 0.5, 1, 1.5, 2, 5$ (Run 1-6).

temperature anisotropies. In particular, higher turbulence level produces excursions in the distribution to higher values of anisotropy. A consistent interpretation of the above results is that the turbulent dynamics produces variations in kinetic anisotropies (measured here by $T_{\perp}/T_{\|}$ and $\beta_{\|}$) even when the global average values are prescribed. Furthermore, when the global average values of β and $\delta b/B_0$ are varied, the dynamical spreading of local anisotropies ventures into different (and sometimes more distant) regions of the parameter space. Temperature anisotropy effects are therefore seen to be qualitatively similar in the simulations and in solar wind observations, keeping in mind of course that the control over parameters is direct in the former case, and obtained through conditional sampling in the latter. Furthermore, the simulation system is much smaller than the solar wind in terms of ratio of correlation scale to ion inertial length, and in the solar wind the velocity DF is sampled generally on scales larger than the ion skin depth.

5.1. *Intermittency and kinetic effects*

Elevated temperatures and enhanced kinetic anisotropies have been identified near coherent magnetic structures, both in plasma simulations (Servidio et al. 2012; Karimabadi et al. 2013; Wu et al. 2013) and in solar wind observations (Osman et al. 2011, 2012a,b). At this point we may inquire whether the link between extremes of kinetic anisotropies and turbulence properties runs deeper still. The connections between coherent structures and kinetic anisotropy have been established in the solar

https://doi.org/10.1017/S0022377814000841 Published online by Cambridge University Press

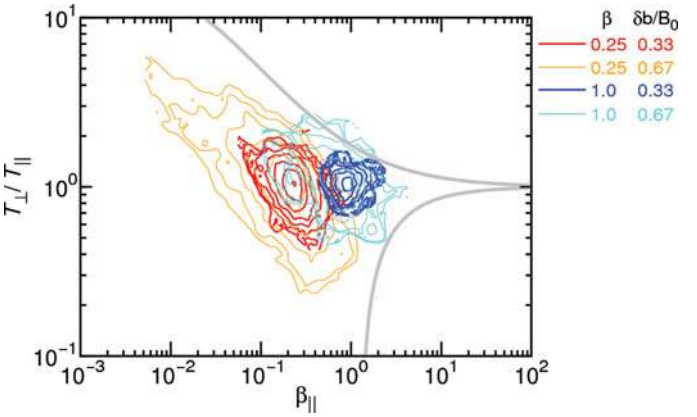

FIGURE 9. Distributions of $T_\perp/T_\parallel$ versus $\beta_\parallel$, comparing simulations with $(\beta, \delta b/B_0) = (0.25, 1/3)$ (thick-red) and $(0.25, 2/3)$ (thin-orange) (left region of the plot). In the right region $(\beta, \delta b/B_0) = (1, 1/3)$ (thick-blue) and $(1, 2/3)$ (thin-cyan) are also superposed. Gray thick curves indicate theoretical growth rates for the mirror ($T_\perp/T_\parallel > 1$) and the oblique firehose ($T_\perp/T_\parallel < 1$) instability (Kasper et al. 2002; Hellinger et al. 2006).

wind by Osman et al. (2012b), based on analysis of magnetic fluctuations. However, in plasma turbulence, dynamical couplings may lead to formation of structure in other fields as well, such as velocity field and density. It is reasonable to suppose that these too might be sites of enhanced anisotropic kinetic activity.

Pursuing the above studies, here we employ our simulations to explore the possible association of magnetic, density and velocity gradients with the occurrence of enhanced kinetic effects. As a classic indicator of the intermittency level, we will sample the current density $\boldsymbol{j}$ and the vorticity field $\boldsymbol{\omega} = \nabla \times \boldsymbol{u}$ in the anisotropy diagram. Once data have been binned in the $\beta_\parallel - T_\perp/T_\parallel$ plane, we evaluated the average magnitude of $\langle|\boldsymbol{j}|\rangle$ and $\langle|\boldsymbol{\omega}|\rangle$ in each bin, using each simulation (here brackets indicate bin-averages). Conditional averaging is useful for revealing physical characteristics within a distribution, especially in simulations with controlled parameters. We note that a recent paper (Hellinger and Trávníček 2014) has raised questions about the use of this approach in the solar wind context. However, the present Vlasov simulations entirely lack variations of collisional age and large scale speed that complicate diagnostics in the solar wind.

As can be seen from Fig. 10(a), where $\langle|\boldsymbol{j}|\rangle$ is shown for Run 8 (different runs show similar results), and where also the data distribution has been superposed, the strongest current density are found near the threshold regions. This is in agreement with the solar wind analysis of magnetic coherent structures (Osman et al. 2012b), indicating that intermittency may play a key role near the instability boundaries of the solar wind.

Analogously, we also computed the averaged vorticity, $\langle|\boldsymbol{\omega}|\rangle$, and the results are reported in Fig. 10(b). Vorticity is also very well correlated with anisotropy, being larger near the boundaries. While we are not interested here in developing the interpretation that the limits of the distributions are defined by linear instabilities of a uniform Vlasov plasma, we note that the enhancements in the lower left part of the distributions do not corresponds to any known instabilities as far as we are aware. As described, for example, by Mikhailovskii (1974), several gradient-driven perturbations may occur in neutral plasmas, that may, therefore, be active in a turbulent pattern such the one we are describing. For example, there is a rich variety of inhomogeneous

https://doi.org/10.1017/S0022377814000841 Published online by Cambridge University Press

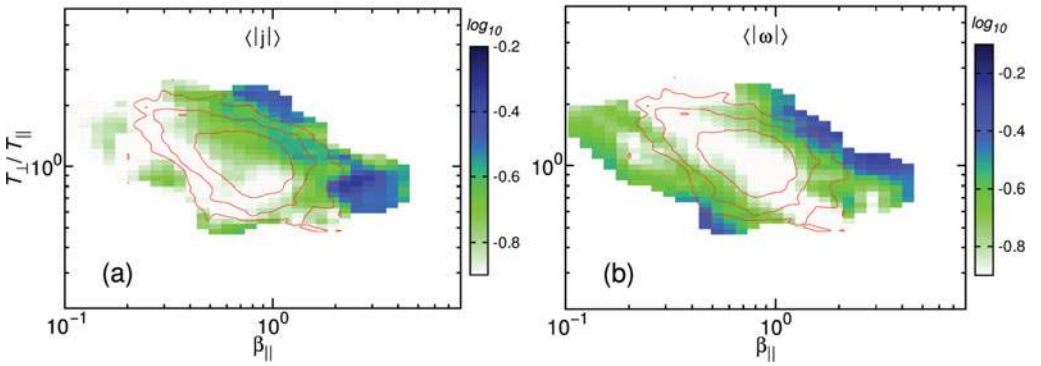

FIGURE 10. (a) Average current density for each bin $\langle |\boldsymbol{j}| \rangle$ in the anisotropy-$\beta_{||}$ plane, for the simulation with $\beta = 1$ and $\delta b/B_0 = 2/3$ (Run 8). (b) Analogously to panel (a), average vorticity $\langle |\boldsymbol{\omega}| \rangle$ for the same simulation. The (red) lines represent the distribution of data points.

instabilities triggered by velocity shears. For a plasma that is embedded in a strong sheared velocity $U(x)$, the growth rate of the instability is $\gamma \sim \zeta \frac{\partial U}{\partial x}$, where ζ is a constant (Mikhailovskii 1974). Obviously the above growth rate is just one case among several possibilities, and may depend upon other parameters (collisionality, angle with the magnetic field, presence of pressure gradients, and so on.) Further investigation is needed on this path.

To generalize these results to solar wind observations, in analogy with previous works on magnetic intermittency (Greco et al. 2008; Greco et al. 2012), we employ a PVI analysis for the examination of several fields. This intermittency measure is given by

$$\mathrm{PVI}_f(s) = \frac{|\Delta \boldsymbol{f}|}{\sqrt{\langle |\Delta \boldsymbol{f}|^2 \rangle}}, \quad \Delta \boldsymbol{f} = \boldsymbol{f}(s + \Delta s) - \boldsymbol{f}(s), \tag{5.1}$$

where $\boldsymbol{f}$ can be the magnetic ($\boldsymbol{b}$) or velocity ($\boldsymbol{u}$) vector field, or the scalar density field (n). The brackets $\langle \ldots \rangle$ denote an appropriate average over many correlation lengths. This is chosen to be the entire simulation box for each simulation (which roughly correspond to 10 h of solar wind observations). The variable s is a 1D spatial coordinate, in analogy with solar wind analysis where it labels the spacecraft sampling time. For the simulation, the local PVI value is computed in both Cartesian directions, averaged and the value assigned to the central point. The statistical distribution of PVI values is very similar to that of the electric current density (see Sec. 6 and Fig. 14, for an example). The results are essentially the same as reported by Greco et al. (2009) who found that PVI distributions in MHD simulations and solar wind are remarkably similar in the inertial range.

The PVI signal in (5.1) has been binned in the plane given by $T_\perp/T_{||} - \beta_{||}$, as described by Osman et al. (2012b). In Fig. 11(a), the PVI of the magnetic field is reported, using the ensemble of all the simulations used in Table 1. Similarly to observations, the ensemble of simulations manifest a condensation of magnetic intermittency near the borders of the distribution, with a particular concentration near the mirror and the oblique firehose instability boundaries, reported here as a reference. To confirm that our results weakly depend on the system size, we also performed the same PVI analysis varying Δs in (5.1) (not shown here), finding

https://doi.org/10.1017/S0022377814000841 Published online by Cambridge University Press

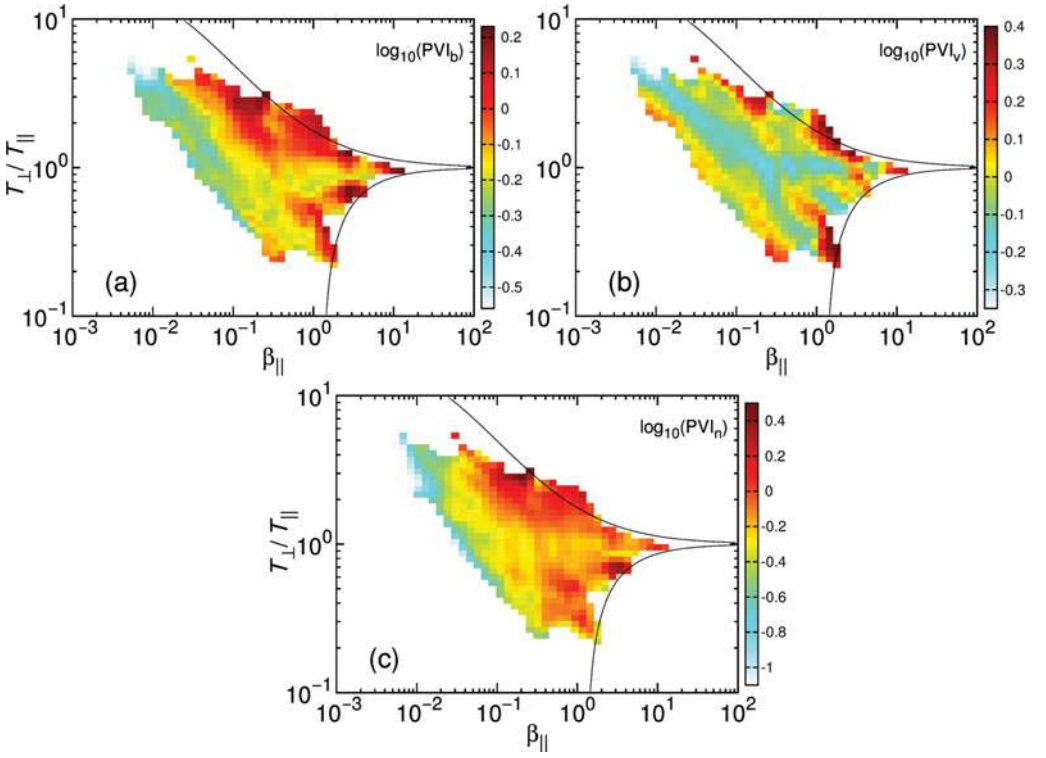

FIGURE 11. Average PVI_f in the anisotropy-$\beta_\parallel$ plane for the ensemble of simulations: PVI_b (a), PVI_u (b) and PVI_n (c). In each panel, dashed curves indicate theoretical growth rates for the mirror ($T_\perp/T_\parallel > 1$) and the oblique fire hose ($T_\perp/T_\parallel < 1$) instability.

essentially that when the sampling rate is in the inertial range of turbulence, the analysis gives similar results.

The same analysis for the velocity field, PVI_u, which is a surrogate for the vorticity of the flow, is reported in Fig. 11(b). As expected from Fig. 10, intermittency of the velocity field is also strongly correlated to temperature anisotropy. The signatures are once again found near the boundaries of the characteristic anisotropy plot. Finally, the bottom panel of Fig. 11 reports the same analyses for PVI_n, an indicator of intermittent structure in the density field. The density results qualitatively resemble both the magnetic and velocity field cases.

A similar analysis was also carried out on 17 years of solar wind data (Servidio et al. 2014), confirming the good analogy between kinetic turbulence and solar wind kinetic effects. The highest values of PVI_f have been found in each case near the extremal regions of the parameter space, and these values are also comparable between simulations and solar wind data. Note that due to the limited number of available simulations, those distributions do not experience parameter excursions as great as those of the solar wind data. One might reason in this way: intermittency is a generic feature of turbulence, leading to coherent structures of increasing sharpness at smaller scales, the effect growing stronger at higher Reynolds numbers (Sreenivasan and Antonia 1997). Stronger fluctuation amplitude is associated with stronger turbulence (e.g. higher Reynolds number, larger cascade rate), and therefore for a plasma, larger $\delta b/B_0$ should be associated with stronger intermittency and stronger small scale coherent

https://doi.org/10.1017/S0022377814000841 Published online by Cambridge University Press

structures. Since coherent structures are connected with kinetic anisotropies, then larger $\delta b/B_0$ should also be connected with stronger anisotropies. This is a variation of the interpretation put forth previously (Bale et al. 2009) that the fluctuation levels are larger near the parameter space boundary regions because instabilities excite these waves (Alexandrova et al. 2013). The explanation for correlations near these boundaries remains an open question. For example, studies such as Smith et al. (2006) show that variance anisotropy (or 'magnetic compressibility') admits correlations with parameters such as normalized turbulence amplitude, and proton beta as expected from theories weakly compressible MHD turbulence. Alternatively (Alexandrova et al. 2013), there has been a suggestion of variance anisotropies in the extremes of beta (and temperature anisotropy) that are attributed to instabilities. We will not pursue these issues further here, but simply remark that in the present interpretation the agency that drives fluctuations and anisotropies near the parameter boundaries is the strong coherent structures generated by turbulence.

6. Multi-ion Vlasov: the role of alpha particles

The interplanetary medium, although predominantly constituted by protons, is also composed by a finite amount of doubly ionized helium (alpha particles), together with a few percents of heavier ions (like oxygen). In order to investigate the complex physics of multi-component solar wind, a fully nonlinear multi-ion Vlasov model is needed. Recently, Perrone et al. (2013a) have performed numerical simulations of the multi-ion plasma, using the HVM code (Valentini et al. 2007; Perrone et al. 2011), in a five-dimensional phase-space configuration. Similarly to the model described in Sec. 2, protons and alpha particles are treated kinetically, and electrons are considered as a fluid, where the generalized Ohm's law retains the Hall effect and the resistive term.

The initial conditions, the simulation setup, and the geometry are the same as the HVM simulations presented in Secs 2, 4 and 5. In particular, the range of parameters is the same as Run 5. For the alpha particles, realistic values for the solar wind conditions are imposed, with a percentage of alpha particles of $\langle n_\alpha \rangle / \langle n_p \rangle = 5\%$, where subscripts α and p hereafter will refer to helium and protons, respectively. In these simulations, 512^2 grid-points in the two-dimensional spatial domain and 61^3 and 31^3 grid-points in proton and alpha particle three-dimensional velocity domains are used, respectively. More details on the run and the model are provided in Perrone et al. (2013a).

We computed the spectral distribution of energy, for both species. It is worth pointing out that the spectra of proton density and velocity do not present significant differences with respect to the case without helium, revealing that the presence of alpha particles does not disturb significantly proton-turbulence. To make a direct comparison of the dynamical evolution of the two ion species, the left panels of Fig. 12 show the power spectra of bulk velocity of protons and α particles, for two different times, namely $t = 1\Omega_{cp}^{-1}$ (a) and $t = 40\Omega_{cp}^{-1}$ (c). This direct comparison of the dynamical evolution of the two ion species does not display significant differences. As discussed in Perrone et al. (2013a), the spectrum of the proton density (not shown here), at high k's is more populated than the spectrum of alpha particles, possibly related to the fact that the alpha particles are heavier than protons, so their inertia may prohibit excessive fluctuations at small scales.

At the same time of the above spectra, the PDFs of the temperature anisotropy for protons and alpha particles have been computed, and here shown in panels (b)

https://doi.org/10.1017/S0022377814000841 Published online by Cambridge University Press

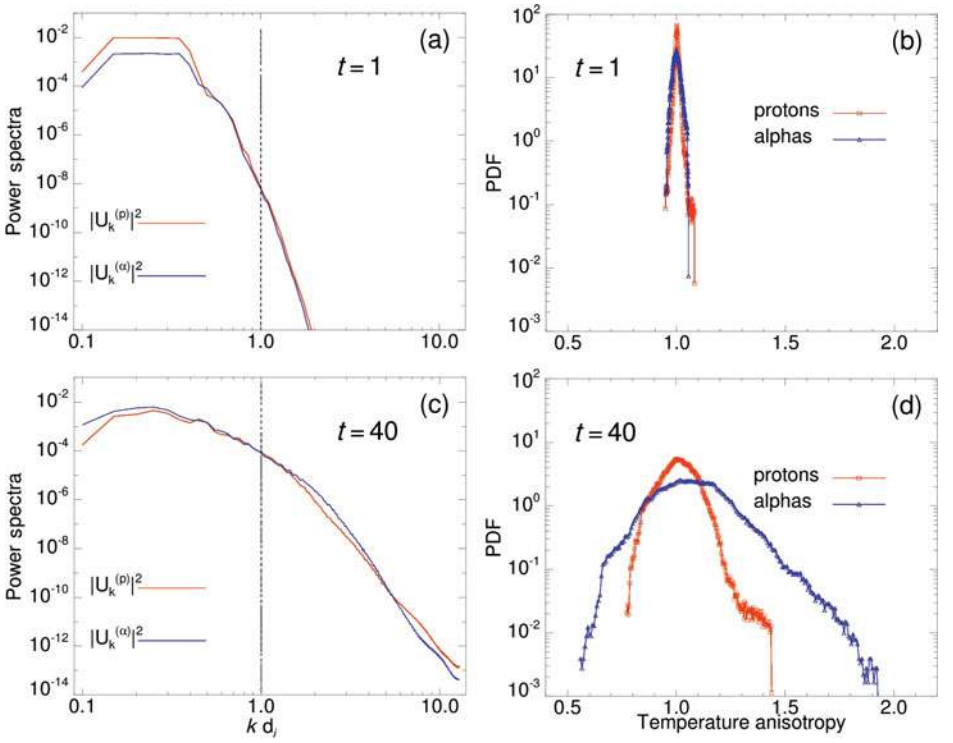

FIGURE 12. Left panels: spectra of the proton (red line) and alpha (blue line) fluid velocity, for $t = 1$ (a) and $t = 40$ (c). Right panels: PDFs of proton (red-square line) and alpha particle (blue-triangle line) anisotropy at the same times of spectra: $t = 1$ (b) and $t = 40$ (d).

and (d) of Fig. 12. This figure clearly indicates that, in the early stage of the system evolution [panels (a) and (b)], when the energy is stored at large scales, the PDFs are narrow and concentrated around the Maxwellian initial condition. During the evolution of the system, when the energy is transferred at small scales through the cascade, the PDFs both elongate in the parallel ($T^i_\perp/T^i_{||} < 1$) and in the perpendicular ($T^i_\perp/T^i_{||} > 1$) direction, displaying a strong anisotropic behavior, that reaches its maximum at $t = 40$ (c)–(d). However, alpha particles are more anisotropic than protons, as commonly observed in space plasmas (Maruca et al. 2012). In agreement with the single-ion HVM model, temperature anisotropy of multiple species appear to be connected with the turbulent cascade.

It is interesting to investigate whether the anisotropy of both species are correlated. Any correlation between $T^p_\perp/T^p_{||}$ and $T^\alpha_\perp/T^\alpha_{||}$ may reveal that simultaneous kinetic instabilities locally occur, modulated by the ambient magnetic field, or that an instability for a given species may influence the other, and vice-versa. The joint probability distribution, shown in Fig. 13, indicates a qualitative correlation between the two ion anisotropies. Although, most of the events are concentrated around $T_\perp/T_{||} \sim 1$, a non-negligible amount of events are broadly scattered because of turbulence. Moreover, a monotonic dependency between alpha and proton anisotropies is recovered, in very good agreement with solar wind observations (Bourouaine et al. 2010, 2011a,b; Maruca et al. 2012). Analogously to Maruca et al.

https://doi.org/10.1017/S0022377814000841 Published online by Cambridge University Press

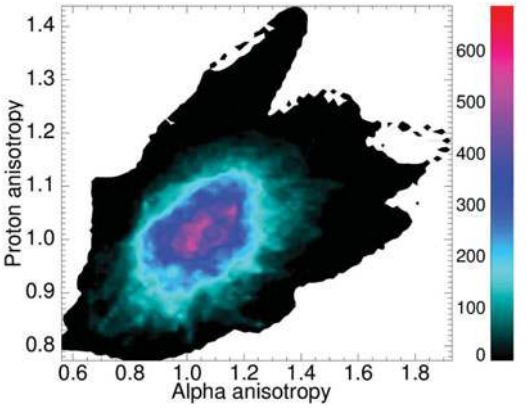

FIGURE 13. Two-dimensional (joint) histogram of proton and alpha particle temperature anisotropy.

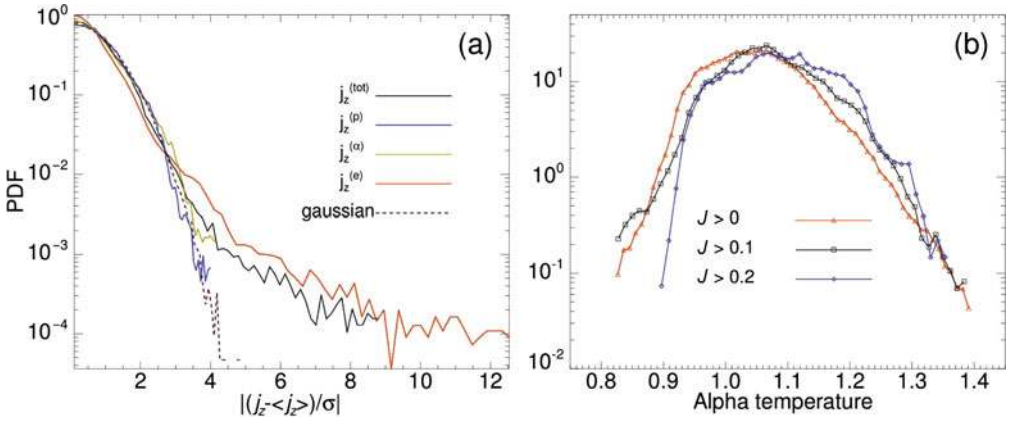

FIGURE 14. (a) PDFs of different current densities in the z-direction using standardized variables. (b) Distributions of alpha temperatures, for three values of the threshold J on the current density.

(2012), we performed a fit of the type

$$\left(\frac{T_\perp^p}{T_{||}^p}\right) \sim \left(\frac{T_\perp^\alpha}{T_{||}^\alpha}\right)^\mu .$$

We obtained $\mu \sim 0.22$, which is in the same range of values as the reference lines drawn by Maruca et al. (2012). This favorable comparison further suggests that the correlation between proton and alpha particle kinetic effects, commonly observed in the solar wind, may be the result of an active turbulent cascade, where kinetic instabilities are locally activated and modulated by the ambient magnetic field and by other non-homogeneous structures.

Analogously to the cases reported in previous sections, the turbulent multi-ion activity leads to the generation of coherent structures and intermittency. To get more insight in this multiple-species intermittency, we computed several contributions to the current density. In particular, we computed the proton current $j_z^{(p)} = Z_p n_p u_z^{(p)}$ (being $Z_p = 1$), the alpha particle current $j_z^{(\alpha)} = Z_\alpha n_\alpha u_z^{(\alpha)}$ and the electron current $j_z^e = j_z^p + j_z^\alpha - j_z$. Panel (a) of Fig. 14 displays the PDFs of the above contributions,

https://doi.org/10.1017/S0022377814000841 Published online by Cambridge University Press

using standardized variables. A Gaussian distribution is also reported for comparison. As it can be seen, while the currents $j_z^{(tot)}$ and $j_z^{(e)}$, related to the gradients of the magnetic field, are highly intermittent, $j_z^{(p)}$ and $j_z^{(\alpha)}$, related to primitive variables of turbulence, show a more Gaussian behavior.

More recently, Perrone et al. (2014) have shown that the presence of these high magnetic stress regions is a signature of *local heating* in the alpha temperature, similarly to proton temperature observations (Osman et al. 2011) and PIC simulations (Wu et al. 2013). Using the present simulation, we briefly report here on the statistics of alpha temperatures conditioned to the thresholds J on the total current density. We investigated three main subranges, conditioning the data in populations that satisfy $J > 0$ (all dataset), $J > 0.1$ and $J > 0.2$ (most intermittent events). In Fig. 14, the conditional temperature PDF of alpha particles shows a clear tendency to increase in samples characterized by higher value of threshold. This result confirms that enhancements of ion temperatures are associated with stronger coherent structures.

7. Magnetic discontinuity analysis

The turbulent solar wind is characterized by broad band electromagnetic fluctuations, that, both in the inertial and in the high frequency range, have been found to be populated by discontinuities. Magnetic discontinuities have been identified as abrupt changes in the plasma and in the magnetic field (Burlaga et al. 1969; Tsurutani and Smith 1979). Historically, the classification of interplanetary discontinuities into categories, such as rotational discontinuities and tangential discontinuities (Wang et al. 2013), has been based on linear ideal MHD theory (Neugebauer 2006). There are also differences in their interpretation: one familiar view is that discontinuities are static boundaries between flux tubes originating in the lower corona (or photosphere). In this 'spaghetti' view, the magnetic tubes may tangle up in space, but remain distinct entities (Mariani et al. 1973). Another interpretation is that some of the observed discontinuities might be the current sheets that form as a consequence of the cascade of MHD turbulence to inertial scales and down (Greco et al. 2009). Since the characteristic thickness of these structures is on the order of the Larmor radius and the ion skin depth (Vasquez et al. 2007) [discontinuities at still smaller scales would be associated with coherent structures at electron kinetic scales (Perri et al. 2012)], a kinetic approach to the study of magnetic discontinuities is needed. In this section, we present a solar wind-like modeling of the magnetic discontinuities, and their relation with the kinetic effects discussed before. In Greco et al. (2012) a statistical analysis has been performed to further quantify the association between distinctive kinetic signatures and intermittent current sheets in the 2D-3V HVM simulations.

Using datasets from Run 5 in Table 1, here we review these results. We performed our analysis at $t^\star$, when the maximum level of turbulent activity is reached. A useful and simple way to systematically identify regions of high magnetic stress and coherent structures is based on statistics of the magnetic field increment vector $\Delta\boldsymbol{b}(s, \Delta s) = \boldsymbol{b}(s + \Delta s) - \boldsymbol{b}(s)$ (Sorriso-Valvo et al. 1999; Bruno et al. 2001). This quantity can be readily calculated along a 1D path s within the 2D simulation box, with a spatial separation (or lag) Δs. Employing only the sequence of magnetic increments, we computed the PVI signal of the magnetic field, described by (5.1). It is related to other measures of coherent structures, such as phase coherence index (Hada et al. 2003) or local intermittency measure (Greco and Perri 2014). For this simulation we choose a small scale lag, $\Delta s \simeq 0.25 d_i$. A sample of the PVI measure along a diagonal path s, that crosses the simulation box several times (Greco et al. 2008), is

https://doi.org/10.1017/S0022377814000841 Published online by Cambridge University Press

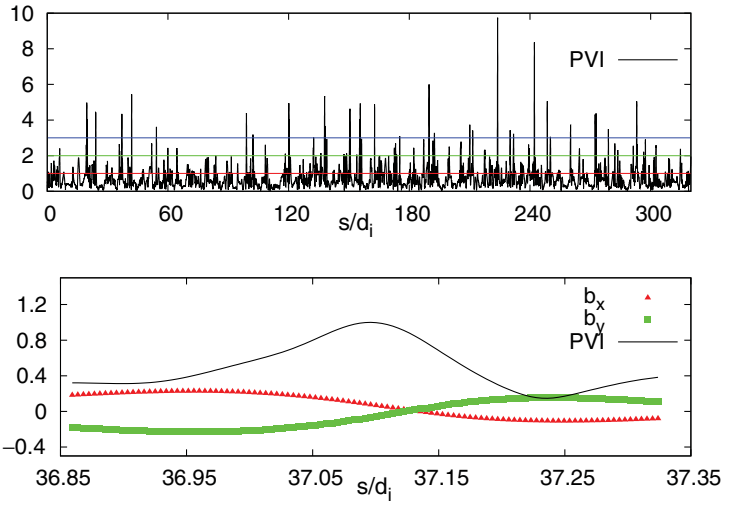

FIGURE 15. (Top) PVI series of the magnetic field, defined by (5.1), obtained by sampling along the trajectory s normalized to the proton skin depth d_i. The thresholds $\theta = 1, 2, 3$ are also shown. (Bottom) Example of discontinuity selected by the PVI method. The two components of the magnetic field vector are displayed along with the PVI signal normalized to its peak value.

shown in the top panel of Fig. 15. Here s is normalized to the proton skin depth d_i. Events such as magnetic discontinuities and regions of high magnetic stress are selected by imposing a threshold on the PVI series, leading to a hierarchy of coherent structures intensities. Indeed, higher and higher values of this threshold correspond to an increase likelihood of finding non-Gaussian inhomogeneous structures. An example of these events is also shown in Fig. 15, where the two in-plane components of the magnetic field are displayed along with the PVI signal.

We examine local kinetic effects associated with inhomogeneous behavior of the magnetic field. To first characterize non-Maxwellian features, we interpolated the proton temperature anisotropy along the 1D path, in order to mimic solar wind data-sampling. As discussed in Sec. 4, in (4.3), a complementary estimate of non-Maxwellian plasma behavior is ϵ, which is a measure of the deviation of the proton distribution from an equivalent Maxwellian. This quantity, defined by (4.3), captures all the higher-order contribution to the non-Maxwellian features. From the spacecraft-like sampling of the magnetic field data along a linear trajectory, discontinuities can be identified by the PVI method with a selected threshold. Figure 16 illustrates the location of discontinuities along the path s, together with shaded contours of ϵ and in-plane magnetic field lines. The figure reveals the association between sheet-like regions of non-Maxwellian behavior (as shown in Fig. 6) and the location of magnetic discontinuities (red open squares).

In order to further investigate these strong local kinetic effects, we have also computed the skewness and the kurtosis of f which represent the third and the fourth moment of the DF respectively. From depicting ϵ, the anisotropy, the skewness $|\boldsymbol{S}|$, and the kurtosis χ_i in the vicinity of a PVI event (not shown), we found that nearby these strongly active regions, anisotropy appears in sheets-like structures. Upstream of these regions a strong heat flux is present. Patterns of χ_i are localized in narrow layers in between magnetic vortexes, where it reveals strong variations from Maxwellian ($\chi_i = 3$). It is clear that, when kinetic effects come into play, the DF f

https://doi.org/10.1017/S0022377814000841 Published online by Cambridge University Press

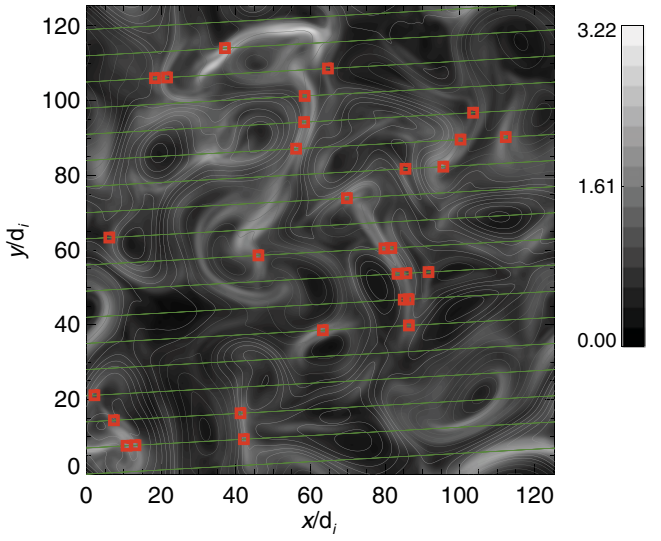

FIGURE 16. Shaded contours of $\epsilon(x, y)$ (in %), defined by (4.3), together with the magnetic flux a_z (grey and white iso-lines). The one dimensional (periodic) path s is also shown (green solid line). The position of the discontinuities identified by PVI technique with threshold $\theta = 3$ (red open squares) are represented. The figure is here adapted from Greco et al. (2012).

departs from the reference Maxwellian g, in concentrated regions of space. The non-Maxwellian features include temperature anisotropy, non-zero skewness (heat flux), or high (low) kurtosis. This has important consequences for the dynamics of plasma turbulence, revealing that these kinetic responses – anisotropy, kurtosis and heat flux – are strongly modulated by local magnetic field structure. The combination of the PVI technique along with direct measurement of non-Maxwellian features shows a strong association of discontinuities and non-Maxwellian features of kinetic origin.

The PDFs of ϵ and temperature anisotropy have been evaluated, conditioned on PVI values: PVI < 1, corresponds to low value fluctuations (increments), $1 <$ PVI < 3 removes low value fluctuations and retains the non-Gaussian structures, and PVI > 3 contains only most highly inhomogeneous structures including current sheets (Greco et al. 2012). Note that the analysis is similar to the one shown in Fig. 14. Panels (a) and (b) of Fig. 17 shows the PDFs of anisotropy and ϵ conditioned on PVI. These plots suggest that the largest and most important distortions of the proton DF occur in the immediate vicinity of discontinuities (PVI > 3) and not in the smoothest regions (PVI < 1). This analysis provide evidence that the 1D solar wind techniques are able to capture the link between strong gradients and non-thermal effects (Osman et al. 2012a,b). The present results add to accumulating evidence that cascade, nonlinearity and associated intermittency, are important in establishing observed kinetic plasma properties in the solar wind, and perhaps more broadly in astrophysical plasmas.

8. Six-dimensional Vlasov turbulence

The use of simplified approaches to the study of solar wind turbulence raised in the past years many interesting discussions (Howes et al. 2008; Matthaeus et al. 2008; Schekochihin et al. 2009; Parashar et al. 2010; Narita et al. 2011; Matthaeus

https://doi.org/10.1017/S0022377814000841 Published online by Cambridge University Press

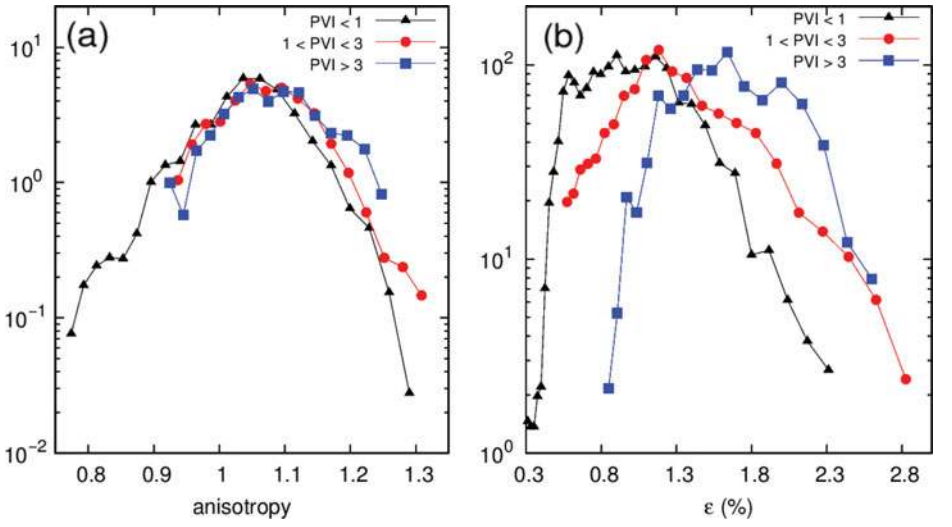

FIGURE 17. Conditioned PDFs of temperature anisotropy (a) and ϵ (b). Conditioning has been performed in three ranges, namely PVI $<$ 1 (black triangles), 1 $<$ PVI $<$ 3 (red bullets) and PVI $<$ 3 (blue squares).

et al. 2014). Reduced models of the Vlasov theory, such as gyrokinetics, are most accurate when the system is strongly magnetized, and perturbations to the equilibrium distribution are very small, let's say, without losing generality, that $\delta b/B_0 \sim \delta f/f_0 \sim \xi \to 0$, where δf are perturbations to a Maxwellian distribution f_0 [for a good review see Schekochihin et al. (2009)]. For the case of space plasmas, however, such restrictions may be violated since fluctuations in a large system can be on the order of the mean field B_0. In order to satisfy the an ergodic theorem, such fluctuations need to be evaluated over scales larger than the correlation length. Theories that are intended for small $\delta b/B$ (Howes et al. 2008; Schekochihin et al. 2009; TenBarge et al. 2013; Howes et al. 2014) are typically applied to small systems, or to the solar wind at small spatial scales only.

In the standard statistical description of turbulence, the ensemble average-range that guarantees convergence of moments is at least a few correlation scales. The latter means that the autocorrelation function of the fluctuations must go to zero at separation scales much smaller than the total size of the turbulent sample (Batchelor 1953; Matthaeus and Goldstein 1982; Lesieur et al. 2001; Dudok de Wit 2004; Matthaeus et al. 2012). When these basic conditions are satisfied, solar wind fluctuations level, even if very spread, shows a majority of datasets that satisfy $0.1 < \delta b/B_0 < 1$. Moreover, as it can be seen from observations, the deviations from the Maxwellian condition can be quite big and non-symmetric, and can give anisotropies that are not $O(\xi)$. These observations have been recovered in the 2.5D + 3V Vlasov simulations, as extensively discussed in the previous sections.

Despite of the good agreement with observations, the 2D Vlasov has been criticized because of the reduced dimensionality in the physical space (although includes three dimensions in the velocity). In particular, it has been objected that 2D spatial variation limits their applicability to turbulent space and astrophysical plasmas for two reasons, namely lack of propagating Alfvénic fluctuations and for the lack of collisionless damping via the usual cyclotron or Landau resonances, that requires variation along the mean magnetic field (TenBarge et al. 2013; Howes et al. 2014). As it is evident

https://doi.org/10.1017/S0022377814000841 Published online by Cambridge University Press

from Fig. 4, the 2.5D system is able to recover some aspects of the incompressive MHD scale cascade, including the near-equipartition of kinetic and magnetic energy (Alfvén effect) and the similar nature of the electric field spectrum. Second, as it can be seen from Sec. 5, the 2.5D system is able to produce the observed anisotropy level.

Similarly to the 2D case, in which a clear link between simulations and observations has been established [see also Servidio et al. (2014)], here we will investigate the full-dimensional Eulerian Vlasov model, with a set of simulations that cover several plasma conditions. We describe here preliminary results of HVM simulations in full 3D-3V phase-space configuration ($3D$ in physical space and $3D$ in velocity space). We simulate a plasma embedded in a uniform background magnetic field, directed along the z-axis ($\boldsymbol{B}_0 = B_0 \boldsymbol{e}_z$). The six-dimensional phase-space is discretized with 128^3 grid points in the spatial domain and 51^3 grid points in the velocity domain. In these conditions, the array containing the particle DF to be evolved in time numerically has a size of $\sim$2.2 TB. Similarly to 2D, equations have been solved in three-periodic Cartesian geometry, with periodicity length $L_{box} = 2\pi \times 20 d_i$ in each direction. For these 3D-3V simulations we used a value of the resistivity $\eta = 2 \times 10^{-3}$. As in the 2D-3V simulations discussed above, the electrons are considered as an isothermal fluid, and the electron to proton temperature ratio is $T_e/T_i = 1$.

At $t = 0$ the plasma has uniform constant density and Maxwellian distribution of velocities. The initial Maxwellian state is perturbed by a 3D isotropic spectrum of fluctuations, for both the magnetic and velocity fields. Initially, excited wave numbers in each direction are chosen, with random phases, in the interval $[1k_0, 5k_0]$, where $k_0 = 2\pi/L_{box}$. The above choice gives a correlation length λ_c which is about 1/5 of the box. No density perturbations are imposed at $t = 0$. The fluctuation level imposed on the system to perturb the initial condition is $\delta b/B_0 = 1/3$, which is a reasonable value for solar wind applications. For a direct comparison with the 2D cases, analogously to Runs in Table 1, we performed six different runs, with $\beta = 0.25, 0.5, 1, 2, 4, 8$. The time step is $\Delta t = 5 \times 10^{-3}$, and the simulations conserves invariant with very good precision, as in the 2D case. The conservation of the total mass, energy and entropy of the system is satisfied with typical relative errors of $\sim 10^{-3}\%$, $3 \times 10^{-1}\%$ and $4 \times 10^{-1}\%$, respectively.

The current density $\boldsymbol{j}$ has been calculated for all the 3D HVM runs, and an example of the magnitude of the current is reported in Fig. 18(a). The shaded 3D contours reveal that the current is strongly intermittent and localized in typical 3D current sheets. As for the fluid models (Uritsky et al. 2010; Zhdankin et al. 2013), these current sheets have three main characteristic lengths, being strongly anisotropic. They indeed look like pancake-like structures, with typical perpendicular (smallest) size on the order of the ion skin depth and parallel elongation (along z) on the order of the parallel correlation length. As we will see, these anisotropic current sheets modulate also the patterns of non-Maxwellian effects such as the temperature anisotropy. In the same Fig. 18, the reduced spectrum of the magnetic fluctuations (reduced in the parallel direction) is reported. Although, the resolution of the simulation is too limited for a characterization of the inertial range (Matthaeus et al. 2008), it can be seen that at scales larger than the proton skin depth the spectrum is consistent with typical theoretical expectations of fluid turbulence.

We point out that in order to fully describe the transition of plasma turbulence at scales much smaller than the proton scales, full kinetic Vlasov (kinetic protons and electrons) simulations, with one or more orders magnitude in resolution, are needed. Although this resolution is unfeasible with the present computational resources, the turbulent fluctuations shown here can initiate non-thermal effects which are

https://doi.org/10.1017/S0022377814000841 Published online by Cambridge University Press

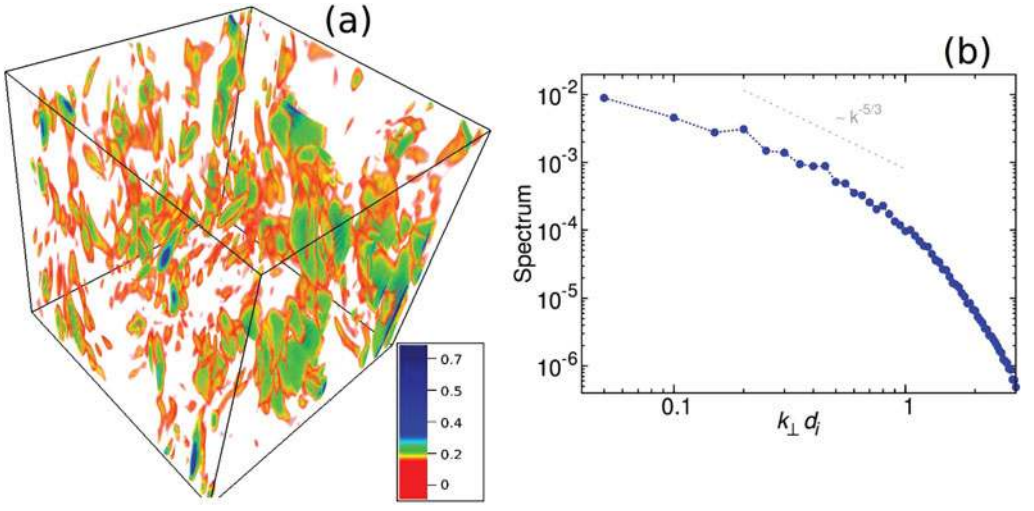

FIGURE 18. (a) 3D shaded contour of the current density $|\boldsymbol{j}|$ for a six-dimensional HVM simulation. As for fluid models, strong current sheets characterize the turbulent pattern. (b) Reduced spectrum of the total magnetic field as a function of $k_\perp d_i$. The dashed (gray) line represents a reference for the eye, indicating the Kolmogorov prediction of turbulence. The case reported is for $\beta = 0.5$ and $\delta b/B_0 = 1/3$.

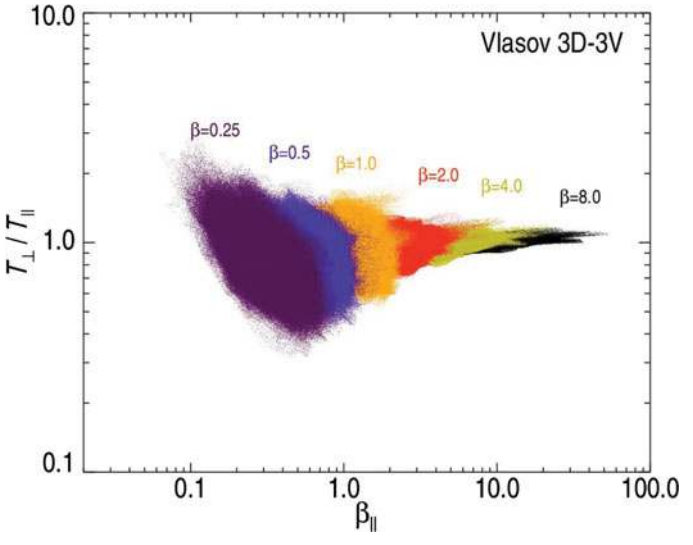

FIGURE 19. Scatter plot of anisotropy $T_\perp/T_\parallel$ versus $\beta_\parallel$ for the 6D HVM simulations, performed with $\delta b/B_0 = 1/3$, and varying $\beta = 0.25$, 0.5, 1, 2, 4, and 8 (from left to right).

comparable to the one observed in the solar wind, producing complex 3D structures in the velocity space. In analogy with the 2D-3V runs, indeed, we computed the temperature anisotropy $T_\perp/T_\parallel$ in the three-dimensional turbulent pattern. In Fig. 19 we report a scatter plot of $T_\perp/T_\parallel$ versus $\beta_\parallel$, at a fixed time (close to the time at which system reaches the maximum peak of nonlinear activity). The different shading of the plot represent runs with different values of the global plasma beta. The results reported in Fig. 19 show that the dynamically evolved distribution of $T_\perp/T_\parallel$ strongly

https://doi.org/10.1017/S0022377814000841 Published online by Cambridge University Press

depends on the particular choice of β (note that at $t = 0$, $T_\perp/T_\parallel = 1$). The picture if very similar to Fig. 8(b). In Fig. 20, the three-dimensional contours of current density and anisotropy are shown, in a region of high anisotropy ($T_\perp/T_\parallel > 1.5$), for the simulation with $\beta = 0.5$. The current density $|\boldsymbol{j}|$ is reported with isosurfaces, while the anisotropy $T_\perp/T_\parallel$ is represented with a transparent shading. As it can be seen, the regions of temperature anisotropy are localized in the general vicinity of elongated current sheets, in agreement with observations (Osman et al. 2012a,b), and 2D simulations (Servidio et al. 2012; Servidio et al. 2014). From these preliminary analysis it seems that also the patterns of temperature anisotropy are anisotropic also in space, being elongated along the magnetic axis.

To conclude this preliminary overview on the 6D results, we now inspect the behavior of the velocity DF in 3V, in a point of high anisotropy. In particular, in Fig. 21, the DF is reported at $(x, y, z) = (55, 78, 74)d_i$, which is located within the box shown in Fig. 20. In the same figure, the pointwise magnetic field is also reported, showing how the DF is affected by its direction, which clearly departs from mean magnetic axis (z). As it can be seen from this 3D representation, many features are present in the DF, with the more pronounced formation of particle beams, due possibly ion-cyclotron interactions (Gary 1993; Marsch et al. 2004; Marsch 2006). The formation of two opposite beams is due to the presence of initial Alfvénic fluctuations that propagate in both directions with respect to the mean magnetic field. Note, indeed, that an isotropic initial spectrum has been chosen, both in variances and in the k space. Form Fig. 21(f), moreover, where the main plane of anisotropy is reported, is evident that strong anisotropy is present, with $T_\perp/T_\parallel \sim 2$, together with non-gyrotropic modulations, due to several possible (and simultaneous) kinetic resonances. In particular, Landau resonances may be locally excited at frequencies that satisfy $\omega - k_\parallel v_\parallel - n\Omega_{ci} = 0$, where $n = 0, 1, \ldots$ (Kennel and Engelmann 2008; Valentini et al. 2008). The above modulations, together with the beam ($n = 0$), can be observed in Fig. 21(f). The full resolution of the velocity space seems to be a very important requirement. We emphasize that any direct linear theory treatment of full-dimensional plasma turbulence must be taken with prudence (Matthaeus et al. 2014).

9. Discussions and conclusions

A model of turbulence has been proposed to investigate kinetic processes in a turbulent plasma, with particular attention to solar wind and astrophysical applications. Using direct numerical simulations of an Eulerian kinetic model, a link between turbulence and non-Maxwellian effects has been established. Recent results in the framework of Vlasov turbulence are reviewed. In particular, it has been found that during the turbulent regime kinetic effects manifest via strong deformations of the proton DF. These patterns of non-Maxwellian features are concentrated in space near regions of strong magnetic activity. A statistical description of the link between the magnetic skeleton of turbulence and the velocity sub-space of the DF has been performed. Although the local magnetic field provides on average the two main directions, a significant population is present at all the angles, suggesting that the main axes of f are determined by the magnetic field in a more complex way. These results underline some possible restrictions in imposing the magnetic field as the unique direction of deformation, and suggest that the commonly observed anisotropy, in which also the bi-Maxwellian approximation is also assumed, gives an underestimation of the real level of anisotropy. Kinetic processes are investigated also

https://doi.org/10.1017/S0022377814000841 Published online by Cambridge University Press

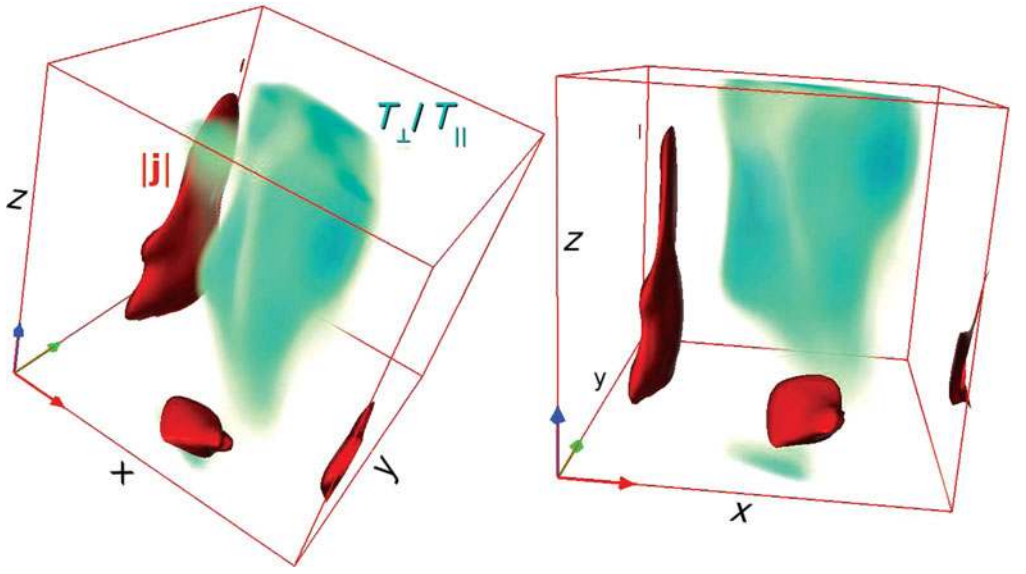

FIGURE 20. 3D contour of current density and anisotropy, in a region of high anisotropy ($T_\perp/T_{||} > 1.5$), from two different perspectives. The current density $|\boldsymbol{j}|$ is reported with (red) isosurfaces, while the anisotropy $T_\perp/T_{||}$ is represented with (azure) transparent fog. The dimensions of the box are $\sim 25 d_i$. Strong anisotropy events are localized in the general vicinity of current sheets.

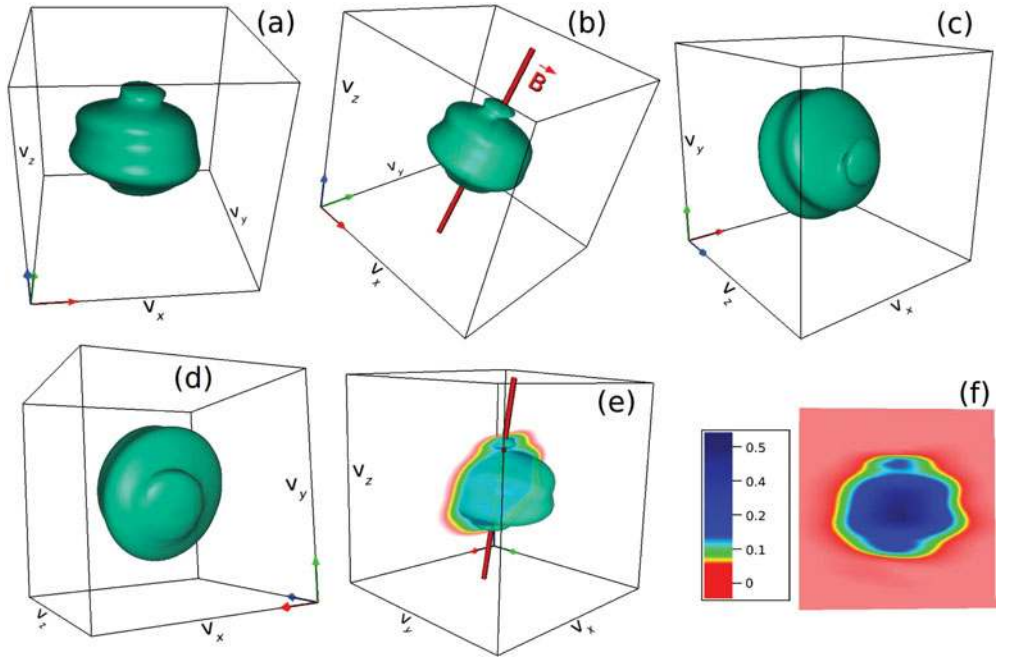

FIGURE 21. Three-dimensional velocity DF for the 6D HVM simulation, at the position $(x, y, z) \sim (55, 78, 74) d_i$, from different perspectives. The distribution is shown at a point of high anisotropy, within the region of Fig. 20. In panel (b) and (e), the local magnetic field is reported as a solid-thick (red) tube. In panel (f) the main plane of anisotropy is reported, where is evident the production of beams, anisotropy, and strong non-gyrotropic modulations.

https://doi.org/10.1017/S0022377814000841 Published online by Cambridge University Press

in the contest of magnetic reconnection, being the latter an element of turbulence itself.

A series of five-dimensional (2D in space and 3D in the velocity space) numerical experiments have been employed to recover temperature anisotropy phenomena, commonly observed in the solar wind. Statistical analysis of spacecraft observations indeed relates proton temperature anisotropy $T_\perp/T_\parallel$ and parallel plasma beta $\beta_\parallel$, where subscripts refer to the local magnetic field direction. This relationship is here recovered using an ensemble of HVM simulations. By varying plasma parameters, such as plasma beta and fluctuation level, the simulations explore distinct regions of the parameter space given by $T_\perp/T_\parallel$ and $\beta_\parallel$, similarly to solar wind sub-datasets. Moreover, both simulation and solar wind data suggest that temperature anisotropy is not only associated with magnetic intermittent events, but also with gradient-type structures in the flow and in the density. It seems increasingly clear that significant kinetic effects including heating have strong association with coherent structures and with the turbulent cascade that produces intermittency. Vlasov hybrid simulations have the advantage that the collisionless kinetic behavior of protons is represented without the counting-statistics issues, contrary to the PIC approach. This advantage is of specific relevance to the present study, because of the association between non-Maxwellian features and small scale intermittency.

The role of alpha particles has been investigated using multi-ion kinetic simulations of turbulence. Both species have been treated kinetically, and it has been found that alpha particles are more anisotropic than protons, as commonly observed in space plasmas. In agreement with observations, moreover, a monotonic dependency between alpha and proton anisotropies has been recovered, indicating the presence of several correlations in turbulence, with the particular development of multi-species intermittency.

The techniques presented here have been used in 1D spacecraft-like analysis, suggesting several possible solar wind applications. The stronger observed temperature anisotropies seen here near high PVI current structures are also compatible with recent solar wind observational studies. For example, computation of the distribution of proton temperatures conditioned on PVI threshold using solar wind spacecraft data reveals that higher PVI samples and therefore coherent magnetic structures are hotter (Osman et al. 2011, 2012a). More detailed study reveals that extremes of proton temperature anisotropy are associated with higher average PVI (Osman et al. 2012b). It is clear that the association of high PVI structures with proton kinetic effects can be established in both cases. This connection between non-Maxwellian kinetic effects and various types of intermittency may be a key point for understanding the complex nature of plasma turbulence. This departure from local thermodynamic equilibrium triggers several processes commonly observed in many astrophysical and laboratory plasmas, especially in cases in which $\delta b/B_0 \neq O(\xi)$. In the latter case, the most complete approach to the study of kinetic turbulence in the collisionless limit remains the full-dimensional Vlasov treatment.

In the present work, we found that the full 3V treatment (3D in the velocity space) of the velocity DF is a crucial requirement for a more complete description of plasma turbulence. From 6D preliminary results we found that: (1) Spectra are consistent with expectation of inertial range turbulence; (2) even for small fluctuation level, $\delta b/B = 1/3$, temperature anisotropy can experience large deviation from the Maxwellian conditions; (3) structures of the temperature anisotropy patterns are obviously more complex than the 2D case, but they are correlated with the intermittent coherent structures, as for the 2D case; (4) with respect to the 2D case, velocity

https://doi.org/10.1017/S0022377814000841 Published online by Cambridge University Press

DFs manifest a more clear production of proton beams, evidencing the role of kinetic resonances; (5) The DF is moreover strongly anisotropic, non-gyrotropic, and with the main axis not generally aligned with the average magnetic field B_0. These preliminary results provide support for several previously reported studies based on 2.5D simulations, confirming several basic conclusions. A much more comprehensive analysis of the comparison between 2D and 3D Vlasov will be performed in future works.

As any model of turbulence, the present approach has some limitations. For example, electron inertia terms are not described by the present HVM model. Even if sophisticated closures for the fluid electrons could be imposed, with the currently employed resolutions very small scale solar wind turbulence may not be adequately described. On the other hand, we can properly describe the kinetic physics at scales much bigger than the electron skin depth. The results reviewed in this work open a new path on the study of kinetic processes such as heating, particle acceleration, and temperature anisotropy, commonly observed in astrophysical and laboratory plasmas. Note that to obtain the above statistical evidence, in both 2D and 3D, one must satisfy some basic requirements. In particular, to guarantee the condition of homogeneity, the size of the turbulent pattern L must be several correlation lengths, namely the correlation scale (or energy containing scale) λ_c must be much bigger than the ion skin depth d_i, and both must be much smaller than the system size. In our case, these conditions are fully satisfied. Having, for example, $L \sim \lambda_c \sim d_i$ would necessary violate these classical requirements, and would be unphysical for solar wind applications, where the separation of scales is enormous.

Acknowledgements

Numerical simulations have been performed on the Fermi supercomputer at CINECA (Bologna, Italy), within the European project PRACE Pra04-771. We acknowledge the 'Turboplasmas' project (Marie Curie FP7 PIRSES-2010-269297), the POR Calabria FSE 2007/2013, the US NSF SHINE (AGS 1156094) and Solar Terrestrial (AGS-1063439) programs and the NASA Heliophysics Grand Challenges program.

REFERENCES

Alexandrova, O., Carbone, V., Veltri, P. and Sorriso-Valvo, L. 2008 Small-scale energy cascade of the solar wind turbulence. *Astrophys. J.* **674**, 1153.

Alexandrova, O., Chen, C. H. K., Sorriso-Valvo, L., Horbury, T. S. and Bale, S. D. 2013 Solar wind turbulence and the role of ion instabilities. *Space Sci. Rev.* **178**, 101.

Alexandrova, O., Saur, J., Lacombe, C., Mangeney, A., Mitchell, J., Schwartz, S. J. and Robert, P. 2009 Universality of solar-wind turbulent spectrum from MHD to electron scales. *Phys. Rev. Lett.* **103**, 165 003.

Araneda, J. A., Maneva, Y. and Marsch, E. 2009 Preferential heating and acceleration of α particles by Alfvén-Cyclotron waves. *Phys. Rev. Lett.* **102**, 175 001.

Araneda, J. A., Marsch, E. and Viñas, A. F. 2008 Proton core heating and beam formation via parametrically unstable Alfvén-Cyclotron waves. *Phys. Rev. Lett.* **100**, 125 003.

Bale, S. D., Kasper, J. C., Howes, G. G., Quataert, E., Salem, C. and Sundkvist, D. 2009 Magnetic fluctuation power near proton temperature anisotropy instability thresholds in the solar wind. *Phys. Rev. Lett.* **103**, 211 101.

Bale, S. D., Kellogg, P. J., Mozer, F. S., Horbury, T. S. and Réme, H. 2005 Measurement of the electric fluctuation spectrum of magnetohydrodynamic turbulence. *Phys. Rev. Lett.* **94**, 215 002.

Batchelor, G. K. 1953 *The Theory of Homogeneous Turbulence*, Cambridge: Cambridge University Press.

Birdsall, C. K. and Langdon, A. B. 1985 *Plasma Physics via Computer Simulation*. New York: McGraw-Hill.

Birn, J. et al. 2001 Geospace environmental modeling (GEM) magnetic reconnection challenge. *J. Geophys. Res.* **106**, 3715.

Biskamp, D. 2000 *Magnetic Reconnection in Plasmas*. Cambridge: Cambridge University Press.

Biskamp, D. 2003 *Magnetohydrodynamic Turbulence*. Cambridge: Cambridge University Press.

Bourouaine, S., Marsch, E., and Neubauer, F. M. 2010 Correlations between the proton temperature anisotropy and transverse high-frequency waves in the solar wind. *Geophys. Res. Lett.* **37**, L14 104.

Bourouaine, S., Marsch, E. and Neubauer, F. M. 2011a On the relative speed and temperature ratio of solar wind alpha particles and protons: collisions versus wave effects. *Astrophys. J. Lett.* **728**, L3.

Bourouaine, S., Marsch, E., and Neubauer, F. M. 2011b Temperature anisotropy and differential streaming of solar wind ions. Correlations with transverse fluctuations. *Astron. Astrophys.* **536**, A39.

Breech, B., Matthaeus, W. H., Minnie, J., Bieber, J. W., Oughton, S., Smith, C. W. and Isenberg, P. A. 2008 Turbulence transport throughout the heliosphere. *J. Geophys. Res.* **113**, A08 105.

Bruno, R. and Carbone, V. 2005 The solar wind as a turbulence laboratory. *Living Rev. Solar Phys.* **2**, 4.

Bruno, R., Carbone, V., Veltri, P., Pietropaolo, E. and Bavassano, B. 2001 Identifying intermittency events in the solar wind. *Planet. Space. Sci.* **49**, 1201.

Burlaga, L. F. 1969 Directional discontinuities in the interplanetary magnetic field. *Solar Phys.* **7**, 54.

Camporeale, E. and Burgess, D. 2011 The dissipation of solar wind turbulent fluctuations at electron scales. *Astrophys. J.* **730**, 114.

Chandran, B. D. G., Li, B., Rogers, B. N., Quataert, E. and Germaschewski, K. 2010 Perpendicular ion heating by low-frequency Alfvén-wave turbulence in the solar wind. *Astrophys. J.* **720**, 503.

Chen, C. Z. and Knorr, G. 1976 The integration of the Vlasov equation in configuration space. *J. Comput. Phys.* **22**, 330.

Cranmer, S. R., Field, G. B. and Kohl, J. L. 1999 Spectroscopic constraints on models of ion cyclotron resonance heating in the polar solar corona and high-speed solar wind. *Astrophys. J.* **518**, 937.

Daughton, W., Roytershteyn, V., Karimabadi, H., Yin, L., Albright, B. J., Bergen, B. and Bowers, K. J. 2011 Role of electron physics in the development of turbulent magnetic reconnection in collisionless plasmas. *Nature Phys.* **7**, 539.

Davidson, R. C. 1990 *Physics of Nonneutral Plasmas*. Redwood City, CA, USA: Addison-Wesley.

Dendy, R. O. and Chapman, S. C. 2006 Characterization and interpretation of strongly nonlinear phenomena in fusion, space and astrophysical plasmas. *Plasma Phys. Control. Fusion* **48**, B313.

Dendy, R. O., Chapman, S. C. and Paczuski, M. 2007 Fusion, space and solar plasmas as complex systems. *Plasma Phys. Control. Fusion* **49**, A95.

Dmitruk, P., Matthaeus, W. H. and Seenu, N. 2004 Test particle energization by current sheets and nonuniform fields in magnetohydrodynamic turbulence. *Astrophys. J.* **617**, 667.

Dobrowolny, M., Mangeney, A. and Veltri, P. 1980 Fully developed anisotropic hydromagnetic turbulence in interplanetary space. *Phys. Rev. Lett.* **45**, 144.

Donato, S., Servidio, S., Dmitruk, P., Carbone, V., Shay, M. A., Cassak, P. A. and Matthaeus, W. H. 2012 Reconnection events in two-dimensional Hall magnetohydrodynamic turbulence. *Phys. Plasmas* **19**, 092 307.

Drake, J. F., Opher, M., Swisdak, M. and Chamoun, J. N. 2010 A magnetic reconnection mechanism for the generation of anomalous cosmic rays. *Astrophys J.* **709**, 963.

Dudok de Wit, T., T. 2004 Can high-order moments be meaningfully estimated from experimental turbulence measurements? *Phys. Rev. E* **70**, 055 302.

Frisch, U. 1995 *Turbulence*. Cambridge: Cambridge University Press.

Galtier, S. and Buchlin, E. 2007 Multiscale hall-magnetohydrodynamic turbulence in the solar wind. *Astrophys. J.* **656**, 560.

Gary, S. P. 1993 *Theory of Space Plasma Microinstabilities*. Cambridge: Cambridge University Press.
Gary, S. P., Saito, S. and Li, H. 2008 Cascade of whistler turbulence: particle-in-cell simulations. *Geophys. Res. Lett.* **35**, L02 104.
Greco, A., Chuychai, P., Matthaeus, W. H., Servidio, S. and Dmitruk, P. 2008 Intermittent MHD structures and classical discontinuities. *Geophys. Res. Lett.* **35**, L19 111.
Greco, A., Matthaeus, W. H., Servidio, S., Chuychai, P. and Dmitruk, P. 2009 Statistical analysis of discontinuities in solar wind ACE data and comparison with intermittent MHD turbulence. *Astrophys. J. Lett.* **691**, L111.
Greco, A. and Perri, S. 2014 Identification of high shears and compressive discontinuities in the inner heliosphere. *Astrophys. J.* **784**, 163.
Greco, A., Valentini, F., Servidio, S. and Matthaeus, W. H. 2012 Inhomogeneous kinetic effects related to intermittent magnetic discontinuities. *Phys. Rev. E* **86**, 066 405.
Hada, T., Koga, D., and Yamamoto, E. 2003 Phase coherence of MHD waves in the solar wind. *Space Sci. Rev.* **107**, 463.
Hansteen, V. H., Leer, E. and Holzer, T. E. 1997 The role of helium in the outer solar atmosphere. *Astrophys. J.* **482**, 498.
Haynes, C. T., Burgess, D. and Camporeale, E. 2014 Reconnection and electron temperature anisotropy in sub-proton scale plasma turbulence. *Astrophys. J.* **783**, 38.
Hellinger, P., Trávníček, P., Kasper, J. C. and Lazarus, A. J. 2006 Solar wind proton temperature anisotropy: linear theory and WIND/SWE observations. *Geophys. Res. Lett.* **33**, L09 101.
Hellinger, P. and Trávníček, P. M. 2014 Solar wind protons at 1 AU: trends and bounds, constraints and correlations. *Astrophys. J. Lett.* **784**, L15.
Heuer, M. and Marsch, E. 2007 Diffusion plateaus in the velocity distributions of fast solar wind protons. *J. Geophys. Res.* **112**, A03 102.
Hollweg, J. V. and Isenberg, P. A. 2002 Generation of the fast solar wind: a review with emphasis on the resonant cyclotron interaction. *J. Geophys. Res.* **107**, 1147.
Howes, G. G., Dorland, W., Cowley, S. C., Hammett, G. W., Quataert, E., Schekochihin, A. A. and Tatsuno, T. 2008 Kinetic simulations of magnetized turbulence in astrophysical plasmas. *Phys. Rev. Lett.* **100**, 065 004.
Howes, G. G., Klein, K. G. and TenBarge, J. M. 2014 The quasilinear premise for the modeling of plasma turbulence. *ArXiv e-prints*.
Hunana, P., Goldstein, M. L., Passot, T., Sulem, P. L., Laveder, D. and Zank, G. P. 2013 Polarization and compressibility of oblique kinetic Alfvén waves. *Astrophys. J.* **766**, 93.
Karimabadi, H. et al. 2013 Coherent structures, intermittent turbulence, and dissipation in high-temperature plasmas. *Phys. Plasmas* **20**, 012 303.
Kasper, J. C., Lazarus, A. J. and Gary, S. P. 2002 Wind/SWE observations of firehose constraint on solar wind proton temperature anisotropy. *Geophys. Res. Lett.* **29**, 1839.
Kasper, J. C., Lazarus, A. J., and Gary, S. P. 2008 Hot solar-wind helium: direct evidence for local heating by Alfven-cyclotron dissipation. *Phys. Rev. Lett.* **101**, 261 103.
Kennel, C. F. and Engelmann, F. 1966 Velocity space diffusion from weak plasma turbulence in a magnetic field. *Phys. Fluids* **9**, 2377–2388.
Kerr, R. M. 1987 Histograms of helicity and strain in numerical turbulence. *Phys. Rev. Lett.* **59**, 783.
Kiyani, K. H., Chapman, S. C., Khotyaintsev, Y. V., Dunlop, M. W. and Sahraoui, F. 2009 Global scale-invariant dissipation in collisionless plasma turbulence. *Phys. Rev. Lett.* **103**, 075 006.
Laveder, D., Marradi, L., Passot, T. and Sulem, P. L. 2011 Fluid simulations of mirror constraints on proton temperature anisotropy in solar wind turbulence. *Geophys. Res. Lett.* **38**, 17 108.
Laveder, D., Passot, T. and Sulem, P. L. 2013 Intermittent dissipation and lack of universality in one-dimensional Alfvénic turbulence. *Phys. Lett. A* **377**, 1535.
Lesieur, M., Yaglom, A. and David, F. 2001 *New Trends in Turbulence*. Spinger.
Maksimovic, M., Pierrard, V. and Lemaire, J. F. 1997 A kinetic model of the solar wind with Kappa distribution functions in the corona. *Astron. Astrophys.* **324**, 725.
Malaspina, D. M., Newmann, D. L., Willson III, L. B., Goets, K., Kellog, P. J. and Kerstin, K. 2013 Electrostatic solitary waves in the solar wind: evidence for instability at solar wind current sheets. *J. Geophys. Res.* **118**, 591.
Mariani, F., Bavassano, B., Villante, U. and Ness, N. F. 1973 Variations of the occurrence rate of discontinuities in the interplanetary magnetic field. *J. Geophys. Res.* **78**, 8011.

Markovskii, S. A. and Vasquez, B. J. 2011a A short-timescale channel of dissipation of the strong solar wind turbulence. *Astrophys. J.* **739**, 22.

Markovskii, S. A. and Vasquez, B. J. 2011b A short-timescale channel of dissipation of the strong solar wind turbulence. *Astrophys. J.* **739**, 22.

Marsch, E. 2006 Kinetic physics of the solar corona and solar wind. *Living Rev. Solar Phys.* **3**, 1.

Marsch, E., Ao, X.-Z. and Tu, C.-Y. 2004 On the temperature anisotropy of the core part of the proton velocity distribution function in the solar wind. *J. Geophys. Res.* **109**, 4102.

Marsch, E., Muhlhauser, K.-H., Rosenbauer, H., Schwenn, R., and Neubauer, F.-M. 1982 Solar wind helium ions: observations of the Helios solar probes between 0.3 and 1 AU. *J. Geophys. Res.* **87**, 35.

Marsch, E., Schwenn, R., Rosenbauer, H., Muehlhaeuser, K.-H., Pilipp, W. and Neubauer, F. M. 1982 Solar wind protons - three-dimensional velocity distributions and derived plasma parameters measured between 0.3 and 1 AU. *J. Geophys. Res.* **87**, 52.

Maruca, B. A., Kasper, J. C. and Bale, S. D. 2011 What are the relative roles of heating and cooling in generating solar wind temperature anisotropies? *Phys. Rev. Lett.* **107**, 201 101.

Maruca, B. A., Kasper, J. C. and Gary, S. P. 2012 Instability-driven limits on helium temperature anisotropy in the solar wind: observations and linear Vlasov analysis. *Astrophys. J.* **748**, 137.

Matteini, L., Landi, S., Hellinger, P., Pantellini, F., Maksimovic, M., Velli, M., Goldstein, B. E. and Marsch, E. 2007 Evolution of the solar wind proton temperature anisotropy from 0.3 to 2.5 AU. *Geophys. Res. Lett.* **34**, L20 105.

Matteini, L., Landi, S., Velli, M. and Matthaeus, W. H. 2013 Proton temperature anisotropy and magnetic reconnection in the solar wind: effects of kinetic instabilities on current sheet stability. *Astrophys. J.* **763**, 142.

Matthaeus, W. H. and Goldstein, M. L. 1982 Stationarity of magnetohydrodynamic fluctuations in the solar wind. *J. Geophys. Res.* **87**, 10 347.

Matthaeus, W. H., Goldstein, M. L. and Roberts, D. A. 1990 Evidence for the presence of quasi-two-dimensional, nearly incompressible fluctuations in the solar wind. *J. Geophys. Res.* **95**, 20 673.

Matthaeus, W. H. and Montgomery, D. 1980 Selective decay hypothesis at high mechanical and magnetic Reynolds numbers. *Ann. New York Acad. Sci.* **357**, 203.

Matthaeus, W. H. and Montgomery, D. 1981 Nonlinear evolution of the sheet pinch. *J. Plasma Phys.* **25**, 11.

Matthaeus, W. H., Servidio, S. and Dmitruk, P. 2008 Comment on "kinetic simulations of magnetized turbulence in astrophysical plasmas'. *Phys. Rev. Lett.* **101**, 149 501.

Matthaeus, W. H., Servidio, S., Dmitruk, P., Carbone, V., Oughton, S., Wan, M. and Osman, K. T. 2012 Local anisotropy, higher order statistics, and turbulence spectra. *Astrophys. J.* **750**, 103.

Matthaeus, W. H.et al. 2014 Nonlinear and linear timescales near kinetic scales in solar wind turbulence. *ArXiv e-prints*.

Matthews, A. P. 1994 Current advance method and cyclic leapfrog for 2D multispecies hybrid plasma simulations. *J. Comput. Phys.* **112**, 102.

Mikhailovskii, A. B. 1974 Theory of plasma instabilities. In: *Instabilities in an Inhomogeneous Plasma*, Vol. 2. New York: Plenum .

Mininni, P. D. and Pouquet, A. 2009 Finite dissipation and intermittency in magnetohydrodynamics. *Phys. Rev. E* **80**, 025 401.

Narita, Y., Gary, S. P., Saito, S., Glassmeier, K.-H. and Motschmann, U. 2011 Dispersion relation analysis of solar wind turbulence. *Geophys. Res. Lett.* **38**, 5101.

Neugebauer, M. 2006 Comment on the abundances of rotational and tangential discontinuities in the solar wind. *J. Geophys. Res.* **111**, 4103.

Osman, K. T., Matthaeus, W. H., Gosling, J. T., Greco, A., Servidio, S., Hnat, B., Chapman, S. C. and Phan, T. D. 2014 Magnetic reconnection and intermittent turbulence in the solar wind. *Phys. Rev. Lett.* **112**, 215 002.

Osman, K. T., Matthaeus, W. H., Greco, A. and Servidio, S. 2011 Evidence for inhomogeneous heating in the solar wind. *Astrophys. J. Lett.* **727**, L11.

Osman, K. T., Matthaeus, W. H., Wan, M. and Rappazzo, A. F. 2012a Intermittency and local heating in the solar wind. *Phys. Rev. Lett.* **108**, 261 102.

Osman, K. T., Matthaeus, W. H., Hnat, B. and Chapman, S. C. 2012b Kinetic signatures and intermittent turbulence in the solar wind plasma. *Phys. Rev. Lett.* **108**, 261 103.

Parashar, T. N., Servidio, S., Breech, B., Shay, M. A. and Matthaeus, W. H. 2010 Kinetic driven turbulence: structure in space and time. *Phys. Plasmas* **17**, 102 304.

Parashar, T. N., Servidio, S., Shay, M. A., Breech, B. and Matthaeus, W. H. 2011 Effect of driving frequency on excitation of turbulence in a kinetic plasma. *Phys. Plasmas* **18**, 092 302.

Parker, E. N. 1988 Nanoflares and the solar X-ray corona. *Astrophys. J.* **330**, 474.

Perri, S., Goldstein, M. L., Dorelli, L. J. and Sahraoui, F. 2012 Detection of small-scale structures in the dissipation regime of solar-wind turbulence. *Phys. Rev. Lett.* **109**, 191 101.

Perrone, D., Valentini, F., Servidio, S., Dalena, S. and Veltri, P. 2013 Vlasov simulations of multi-ion plasma turbulence in the solar wind. *Astrophys. J.* **762**, 99.

Perrone, D., Valentini, F., Servidio, S., Dalena, S. and Veltri, P. 2014 Analysis of intermittent heating in a multi-component turbulent plasma. *Europhys. J.D.* **68**, 7.

Perrone, D., Valentini, F. and Veltri, P. 2011 The role of alpha particles in the evolution of the solar-wind turbulence toward short spatial scales. *Astrophys. J.* **741**, 43.

Perrone, D. et al. 2013 Nonclassical transport and particle-field coupling: from laboratory plasmas to the solar wind. *Space Sci. Rev.* **178**, 233.

Sahraoui, F., Goldstein, M. L., Belmont, G., Canu, P. and Rezeau, L. 2010 Three dimensional anisotropic k spectra of turbulence at subproton scales in the solar wind. *Phys. Rev. Lett.* **105**, 131 101.

Sahraoui, F., Goldstein, M. L., Robert, P. and Khotyaintsev, Yu. V. 2009 Evidence of a cascade and dissipation of solar wind turbulence at electron scales. *Phys. Rev. Lett.* **102**, 231 102.

Saito, S., Gary, S. P., Li, H. and Narita, Y. 2008 Whistler turbulence: particle-in-cell simulations. *Phys. Plasmas* **15**, 102 305.

Schekochihin, A. A., Cowley, S. C., Dorland, W., Hammett, G. W., Howes, G. G., Quataert, E. and Tatsuno, T. 2009 Astrophysical gyrokinetics: kinetic and fluid turbulent cascades in magnetized weakly collisional plasmas. *Astrophys. J. Suppl.* **182**, 310.

Servidio, S., Carbone, V., Primavera, L., Veltri, P. and Stasiewicz, K. 2007 Compressible turbulence in hall magnetohydrodynamics. *Planet. Space Sci.* **55**, 2239.

Servidio, S., Matthaeus, W. H., Shay, M. A., Cassak, P. A. and Dmitruk, P. 2009 Magnetic reconnection in two-dimensional magnetohydrodynamic turbulence. *Phys. Rev. Lett.* **102**, 115 003.

Servidio, S., Matthaeus, W. H., Shay, M. A., Dmitruk, P., Cassak, P. A. and Wan, M. 2010 Statistics of magnetic reconnection in two-dimensional magnetohydrodynamic turbulence. *Phys. Plasmas* **17**, 032 315.

Servidio, S., Osman, K. T., Valentini, F., Perrone, D., Califano, F., Chapman, S., Matthaeus, W. H. and Veltri, P. 2014 Proton kinetic effects in Vlasov and solar wind turbulence. *Astrophys. J. Lett.* **781**, L27.

Servidio, S., Valentini, F., Califano, F. and Veltri, P. 2012 Local kinetic effects in two-dimensional plasma turbulence. *Phys. Rev. Lett.* **108**, 045 001.

Shay, M. A., Drake, J. F., Denton, R. E. and Biskamp, D. 1998 Structure of the dissipation region during collisionless magnetic reconnection. *J. Geophys. Res.* **103**, 9165.

She, Z.-S., Jackson, E. and Orszag, S. A. 1990 Intermittent vortex structures in homogeneous isotropic turbulence. *Nature* **344**, 226.

Siggia, E. D. 1981 Numerical study of small-scale intermittency in three-dimensional turbulence. *J. Fluid Mech.* **107**, 375.

Smith, C. W., Vasquez, B. J. and Hamilton, K. 2006 Interplanetary magnetic fluctuation anisotropy in the inertial range. *J. Geophys. Res.* **111**, A09 111.

Sonnerup, B. U. O. and Cahill, Jr., L. J. 1967 Magnetopause structure and attitude from explorer 12 observations. *J. Geophys. Res.* **72**, 171.

Sorriso-Valvo, L., Carbone, V., Veltri, P., Consolini, G. and Bruno, R. 1999 Intermittency in the solar wind turbulence through probability distribution functions of fluctuations. *Geophys. Res. Lett.* **26**, 1801.

Sreenivasan, K. R. and Antonia, R. A. 1997 The phenomenology of small-scale turbulence. *Annu. Rev. Fluid Mech.* **29**, 435.

Sundkvist, D., Retinó, A., Vaivads, A. and Bale, S. D. 2007 Dissipation in turbulent plasma due to reconnection in thin current sheets. *Phys. Rev. Lett.* **99**, 025 004.

TenBarge, J. M., Howes, G. G. and Dorland, W. 2013 Collisionless damping at electron scales in solar wind turbulence. *Astrophys. J.* **774**, 139.

Tessein, J. A., Matthaeus, W. H., Wan, M., Osman, K. T., Ruffolo, D., and Giacalone, J. 2013 Association of suprathermal particles with coherent structures and shocks. *Astrophys. J. Lett.* **776**, L8.

Tsurutani, B. T. and Smith, E. J. 1979 Interplanetary discontinuities -temporal variations and the radial gradient from 1 to 8.5 AU. *J. Geophys. Res.* **84**, 2773.

Tu, C.-Y., Marsch, E. and Qin, Z.-R. 2004 Dependence of the proton beam drift velocity on the proton core plasma beta in the solar wind. *J. Geophys. Res. (Space Physics)* **109**, 5101.

Tu, C. -Y., Wang, L. -H. and Marsch, E. 2002 Formation of the proton beam distribution in high-speed solar wind. *J. Geophys. Res.* **107**, 1291.

Uritsky, V. M., Pouquet, A., Rosenberg, D., Mininni, P. D. and Donovan, E. F. 2010 Structures in magnetohydrodynamic turbulence: detection and scaling. *Phys. Rev. E* **82**, 056 326.

Vainshtein, S. I., Du, Y. and Sreenivasan, K. R. 1994 Sign-singular measure and its association with turbulent scalings. *Phys. Rev. E* **49**, 2521.

Valentini, F., Califano, F. and Veltri, P. 2010 Two-dimensional kinetic turbulence in the solar wind. *Phys. Rev. Lett.* **104**, 205 002.

Valentini, F., Perrone, D. and Veltri, P. 2011 Short-wavelength electrostatic fluctuations in the solar wind. *Astrophys. J.* **739**, 54.

Valentini, F., Trávníček, P., Califano, F., Hellinger, P. and Mangeney, A. 2007 A hybrid-Vlasov model based on the current advance method for the simulation of collisionless magnetized plasma. *J. Comput. Phys.* **225**, 753.

Valentini, F. and Veltri, P. 2009 Electrostatic short-scale termination of solar-wind turbulence. *Phys. Rev. Lett.* **102**, 225 001.

Valentini, F., Veltri, P., Califano, F. and Mangeney, A. 2008 Cross-scale effects in solar-wind turbulence. *Phys. Rev. Lett.* **101**, 025 006.

Vasquez, B. J., Abramenko, V. I., Haggerty, D. K., and Smith, C. W. 2007 Numerous small magnetic field discontinuities of Bartels rotation 2286 and the potential role of Alfvénic turbulence. *J. Geophys. Res.* **112**, 11 102.

Vasquez, B. J. and Markovskii, S. A. 2012 Velocity power spectra from cross-field turbulence in the proton kinetic regime. *Astrophys. J.* **747**, 19.

Veltri, P. 1999 MHD turbulence in the solar wind: self-similarity, intermittency and coherent structures. *Plasma Phys. Control. Fusion* **41**, A787.

Vincent, A. and Meneguzzi, M. 1991 The spatial structure and statistical properties of homogeneous turbulence. *J. Fluid Mech.* **225**, 1.

Wang, X., Tu, C., He, J., Marschand, E. and Wang, L. 2013 On intermittent turbulence heating of the solar wind: differences between tangential and rotational discontinuities. *Astrophys. J. Lett.* **772**, L14.

Wu, C. C. and Chang, T. 2000 2D MHD simulation of the emergence and merging of coherent structures. *Geophys. Res. Lett.* **27**, 863.

Wu, P., Perri, S., Osman, K. T., Wan, M., Matthaeus, W. H., Shay, M. A., Goldstein, M. L., Karimabadi, H. and Chapman, S. 2013 Intermittent heating in solar wind and kinetic simulations. *Astrophys. J. Lett.* **763**, L30.

Zhdankin, V., Uzdensky, D. A., Perez, J. C. and Boldyrev, S. 2013 Statistical analysis of current sheets in three-dimensional magnetohydrodynamic turbulence. *Astrophys. J.* **771**, 124.